University of Wrocław

Masters Thesis

Krypton calibration of time projection chambers of the NA61/SHINE experiment

Author:
Michał Naskręt

Supervisor:
Prof. David Blaschke

A thesis submitted in fulfilment of the requirements for the degree of Master of Science

in the

Elementary Particle Theory Group
Institute of Theoretical Physcis

October 12, 2015

"Thanks to my solid academic training, today I can write hundreds of words on virtually any topic without possessing a shred of information, which is how I got a good job..."

Dave Barry

UNIVERSITY OF WROCŁAW

Abstract

Institute of Theoretical Physcis

Master of Science

Krypton calibration of time projection chambers of the NA61/SHINE experiment

by Michał Naskręt

The NA61/SHINE experiment at CERN is searching for the critical point in phase transition between quark-gluon plasma and hadronic matter. To do so we use the most precise apparatus - Time Projection Chamber. Its main task is to find trajectories of particles created in a relativistic collision. In order to improve efficiency of TPCs, we introduce calibration using radioactive krypton gas. Simulation of events in a TPC chamber through a decay of excited krypton atoms gives us a spectrum, which is later fitted to the model spectrum of krypton from a Monte-Carlo simulation. The data obtained in such a way serves us to determine malfunctioning electronics in TPCs. Thanks to the krypton calibration we can create a map of pad by pad gains. In this thesis I will describe in detail the NA61 experimental setup, krypton calibration procedure, calibration algorithm and results for recent calibration runs.

UNIVERSYTET WROCŁAWSKI

Abstrakt

Instytut Fizyki Teoretycznej

Kalibracja kryptonowa komór projekcji czasowej w eksperymencie NA61/SHINE

Michał Naskręt

Celem eksperymentu NA61/SHINE w ośrodku badawczym CERN jest poszukiwanie punktu krytycznego w przejściu fazowym pomiędzy plazmą kwarkowo-gluonową a materią hadronową. W tym celu wykorzystuje się niezwykle precyzyjną aparaturę - komory projekcji czasowej(TPC). Ich głównym zadaniem jest określanie trajektorii lotu cząstek wytwarzanych podczas relatywistycznych zderzeń. Aby zwiększyć skuteczność pracy TPC stosuje się kalibrację przy użyciu radioaktywnego izotopu kryptonu pod postacią gazu. Symulacja zdarzeń poprzez rozpad atomów kryptonu daje nam spektrum, które może być później dopasowane do modelowego spektrum kryptonu z symulacji Monte-Carlo. Dane uzyskane w ten sposób służą do zdeterminowania wadliwej elektroniki w TPC. Dzięki kalibracji kryptonowej tworzymy mapę współczynników wzmacniających lub osłabiających sygnał. W tej pracy opisany zostanie szczegółowo układ eksperymentu, procedura kalibracji kryptonowej, algorytm kalibracyjny oraz wyniki pomiarów kalibracyjnych.

Acknowledgements

During my work on this thesis I received a substantial help from many people. I would like to thank the NA61/SHINE collaboration for countless discussions with many experts, such as prof. Marek Gaździcki, Antoni Aduszkiewicz and András László.

I would also like to thank Andrzej Rybicki, who was leading the Kr calibration process for many years. His knowledge in this subject was very helpful.

Finally I would like to thank my supervisor, prof. David Blaschke, for his mentorship throughout the studies.

Contents

List of Figures

List of Tables

Abbreviations

TPC	**T**ime **P**rojection **C**hamber
MTPC	**M**ain **T**ime **P**rojection **C**hamber
VTPC	**V**ertex **T**ime **P**rojection **C**hamber
GTPC	**G**ap **T**ime **P**rojection **C**hamber
LMPD	**L**ow **M**omemntum **P**article **D**etector
NA61	**N**orth **A**rea experiment number **61**
SHINE	**S**PS **H**eavy **I**on and **N**eutrino **E**xperiment
SPS	**S**uper **P**roton **S**ynchrotron
LHC	**L**arge **H**adron **C**ollider
PS	**P**roton **S**ynchrotron
PSB	**P**roton **S**ynchrotron **B**ooster
LEIR	**L**ow **E**nergy **I**on **R**ing
LINAC	**LIN**ear **AC**celerator

Physical Constants

Speed of Light $c = 2.997\ 924\ 58 \times 10^8\ \mathrm{ms}^{-\mathrm{S}}$ (exact)

Symbols

a	distance	m
P	power	W (Js^{-1})
ω	angular frequency	rads^{-1}

To my. . . self

Chapter 1

Introduction

1.1 The NA61/SHINE experiment at CERN

The NA61/SHINE experiment is located at CERN, the European Organization for Nuclear Research. Its name stands for **S**PS **H**eavy **I**on and **N**eutrino **E**xperiment in the **N**orth **A**rea of the CERN Super Proton Synchrotron. It is a successor of the NA49 experiment, which operated from 1995 until 2002. The NA61/SHINE experiment recorded first data with hadron beams in 2009. It is used in order to study hadron-proton, hadron-nucleus and nucleus-nucleus collisions.

1.1.1 Motivation

The physics goals of the experiment are the following:

- Study of the properties of the onset of deconfinement and search for the critical endpoint in strongly interacting matter,
- Hadron production measurements for neutrino beam flux calculations and cosmic ray air showers simulation.

Matter under extreme conditions such as in heavy ion collisions, forms a phase which is called quark gluon plasma. At high enough collision energy and baryonic chemical potential quarks and gluons are no longer confined in nucleons, but freely move in the volume where appropriate conditions prevail. The evidence for this new state of matter was first observed at CERN in 2000. A number of experiments using the SPS contributed to this discovery, including NA49. The main goal of the NA61/SHINE experiment is to find the critical point in transition between hadronic matter and quark gluon plasma. It

is done through a two-dimensional scan over energy-baryonic density plane. The calendar of NA61/SHINE experiment data taking runs inspecting different areas on the plane is presented on the figure 1.1.

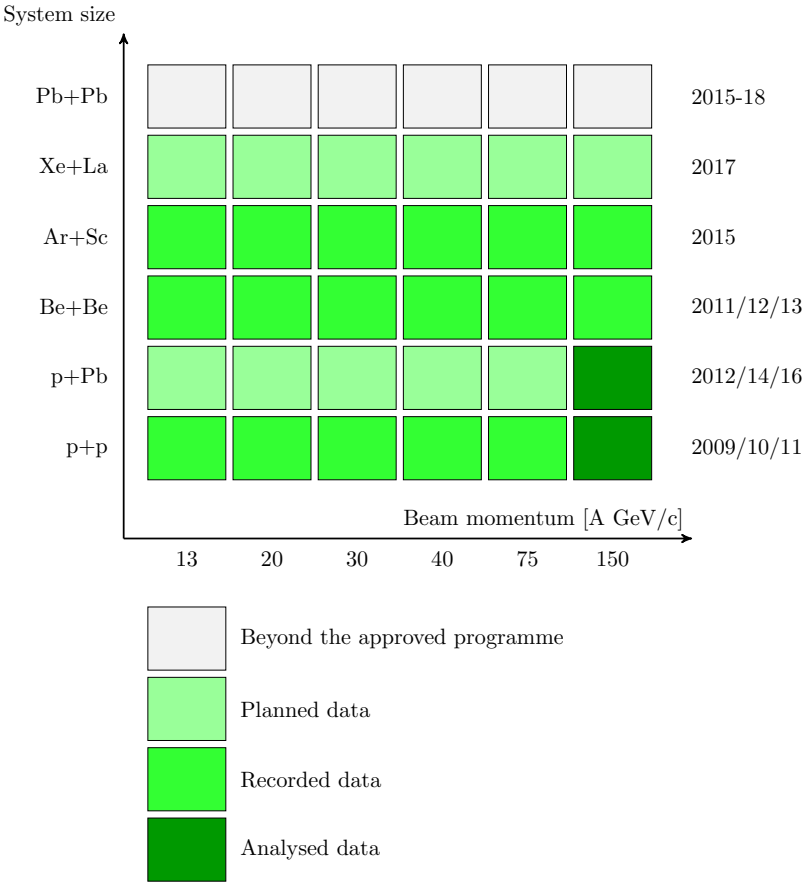

FIGURE 1.1: Calendar of data taking for different energies and system sizes

1.2 Experimental setup

The NA61/SHINE experimental setup consists of a number of detectors. The most important one is the large acceptance hadron spectrometer build up from six Time Projection Chambers and Time-of-Flight detectors. It is used for charged particle momentum measurement and identification. The Projectile Spectator Detector is used to measure the centrality of collision through calculating the non-interacting nucleons energy flow along the beam direction. An array of beam detectors identifies beam particles, secondary hadrons and ions as well as primary ions and measures precisely their trajectories. The schematics of the experimental setup is presented on the figure 1.2.

The description in the following sections is largely based on [1] and [2].

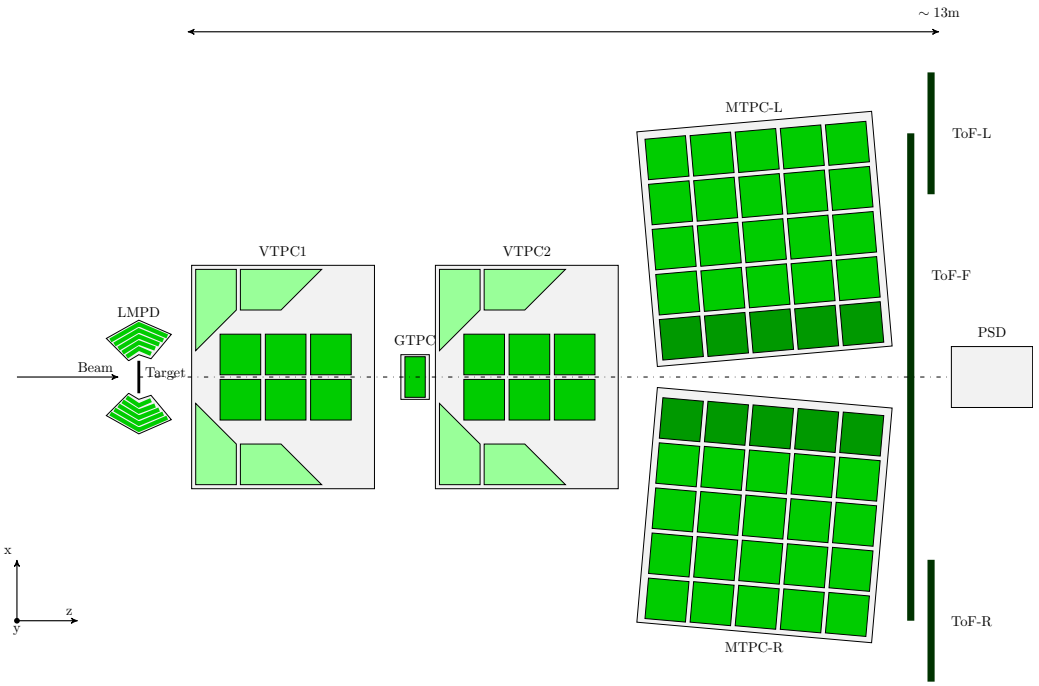

FIGURE 1.2: Overview of the NA61/SHINE experiment. The beam approaches the experiment along the z axis. Trajectory of debris from collision is bent by vertical magnets along x-z axis. The drift direction in the TPC is along the y axis

1.2.1 Beams

The path of beams used in NA61/SHINE begins a few kilometers from CERN North Area - at the biggest CERN site in Meyrin. The schematics of accelerator chain is shown in figure 1.3. The NA61/SHINE experiment uses a number of different beams for its physics programme: protons, lead, beryllium, argon and xenon. Extracted from a source, protons and ions go through a chain of different accelerators in order to obtain expected energy. Protons and other ions follow different paths in their pre-injection chain to Proton Synchrotron.

The proton beam starts its way from a hydrogen source and is first accelerated by LINAC 2 (Linear Accelerator 2). Next, the beam accelerated to 50 MeV is injected into four rings of PSB (Proton Synchrotron Booster). The PSB accelerates the beam up to 1.4 GeV and then transfers it to CERN's oldest accelerator, the PS (Proton Synchrotron). After acceleration to 14 Gev/c the beam is injected into last accelerator ring, the SPS (Super Proton Synchrotron). Here, its energy achieves the highest value of 400 GeV/c.

The path of the ion beam will be presented on an example of lead. The sample of isotopically pure ^{208}Pb is ionized by the Electron Cyclotron Resonance ion source and extracted from the source with energy of 2 keV/u. Then, only atoms ionized 29 times (Pb29+) are selected to enter the LINAC 3. At the exit of LINAC 3 the beam with

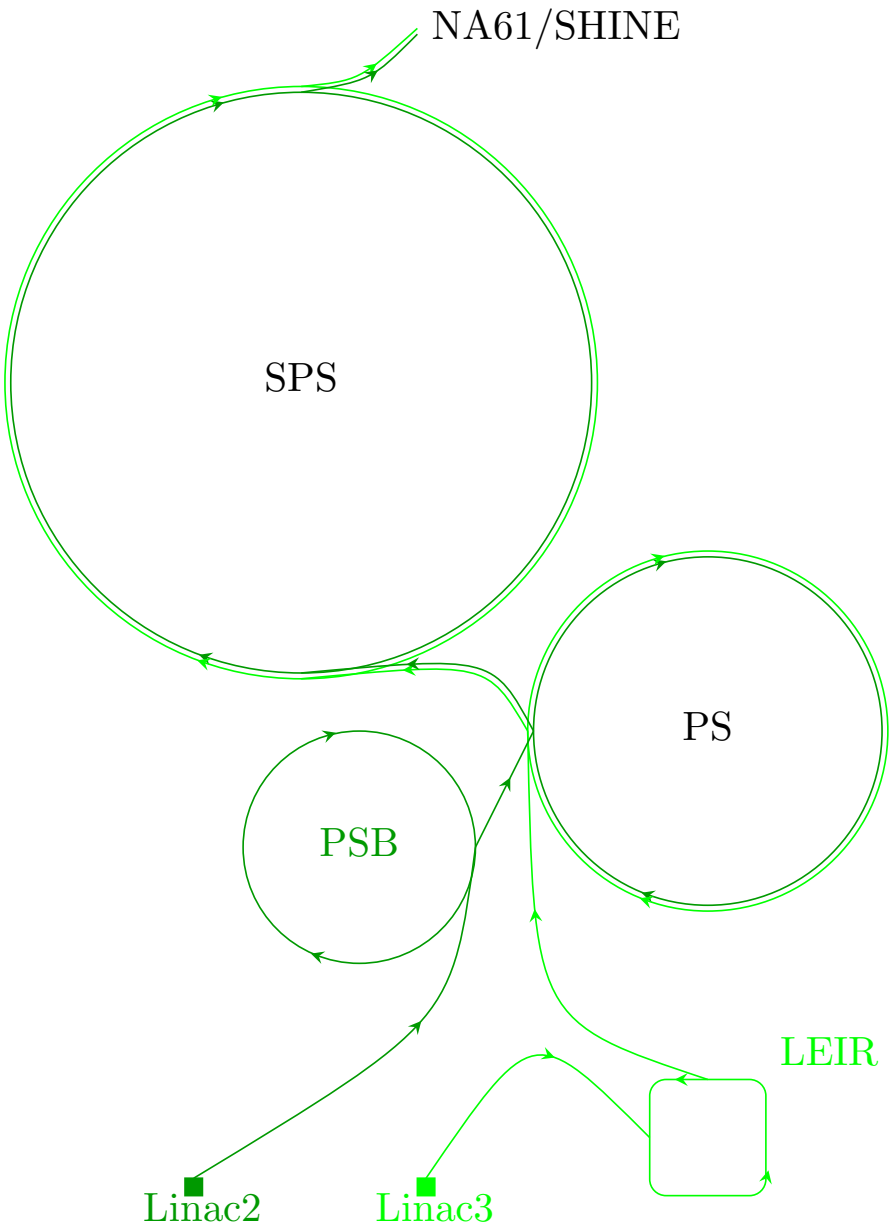

FIGURE 1.3: Top view of the accelerator chain relevant to NA61/SHINE

energy of 4.2 MeV/u is stripped through a carbon foil and the state of Pb54+ is selected by the spectrometer. Then the beam is injected into the LEIR (Low Energy Ion Ring) where it is accelerated up to 72 MeV/u. Next, the beam is accelerated by the PS to 5.9 GeV/u and goes through final stripping to Pb82+ where aluminum foil is used. In the final step, the beam is injected into the SPS where it can achieve energies in the range of $13 - 160$ GeV/u.

The beam from the SPS is directed to one of the branches - H2 beamline. The H2 secondary beamline starts after the T2 primary target. It is capable of transporting momentum selected secondary particles to the EHN1 (Experimental Hall North 1). The

Accelerator	Ions	Protons
LINAC 2	-	50 MeV
LINAC 3	4.2 MeV/u	-
LEIR	72 MeV/u	-
PSB	-	1.4 GeV
PS	5.9 GeV/u	14 GeV/c
SPS	13 – 160 GeV/u	400 GeV/c

TABLE 1.1: List of energies that beams obtain in different accelerators

H2 beamline can transport charged particles in a wide range of momenta, from 9 GeV/c up to maximum SPS momentum of 400 GeV/c. Alternatively, the beamline can transport a primary beam of protons or ions.

1.2.2 Beam detectors and trigger system

A set of detectors is used in order to measure the precise beam position, its intensity and timing. There are also detectors used to determine if interaction with the target has occurred. All of them send triggering signals to other detectors, i.e. TPCs and PSD.

The most important detectors are the beam counters S1, S2, S4 and the BPDs (Beam Position Detectors)

The beam counters S1, S2 and S4 are thin plastic scintillators placed in different distance from the target. The S1(0.5cm thick) and S2(0.2cm thick) are used for precise time of flight measurements. The last scintillator S4 is 0.5cm thick and located behind the target. If there are no particles going through the S4 it means that interaction in target has occurred and the triggering signal is sent to other detectors.

Three Beam Position Detectors are placed along the beamline in order to measure precise beam position in the transverse plane. These detectors are proportional chambers with two orthogonal wire planes sandwiched between three cathode planes. Each BPD measures the position of trigger-selected beam in two orthogonal directions independently.

The trigger system uses information from several detectors for beam particle identification. In order to fulfill requirements of NA61/SHINE physics program it is a flexible and robust system. The system can run simultaneously up to four different triggers which are recorded for offline selection.

1.2.3 Time Projection Chambers

Time Projection Chambers are the core detectors of the NA61/SHINE experiment. They are used for particle tracks reconstruction in three dimensions. There are four large volume TPCs used in the experiment. Two of them are located in a region where magnetic field is applied, these are called Vertex TPCs: VTPC-1 and VTPC-2. Two others are called Main TPCs: MTPC-L and MTPC-R. They are located downstream of the magnets, symmetrically to the beam. Additional small volume TPC is located between two VTPCs, centered on the beamline. It is called GTPC (Gap TPC). Also, the LMPD (Low Momentum Particle Detector) which was installed in 2014, consist of two small TPC chambers and is located around the target. In a single Pb+Pb interaction TPCs allow reconstruction of over 1000 tracks. Up to 234 clusters and samples of energy loss per particle trajectory are sufficient for precise measurements. The overview of TPCs positioning in the experimental setup is drawn in the figure 1.2

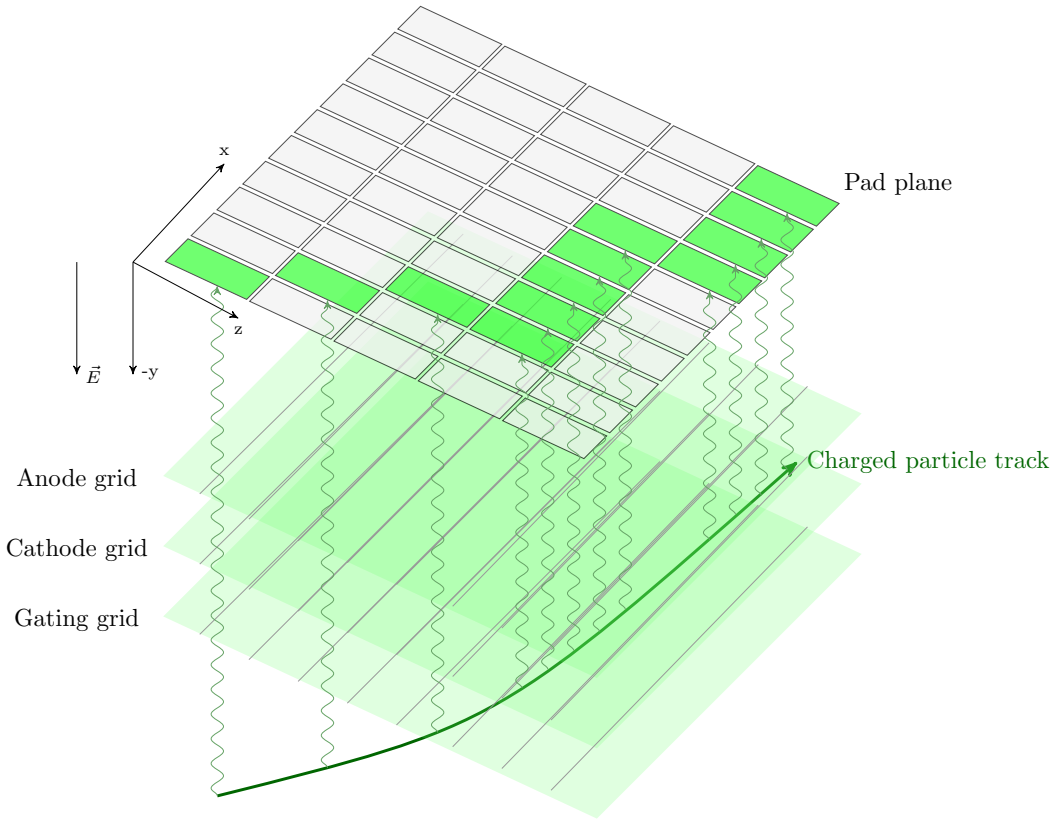

FIGURE 1.4: TPC principle of operation

Figure 1.4 presents the principle of operation of the TPCs. The TPC is a large volume filled with gas mixture of argon and carbon dioxide. When a high-energy charged particle goes through the volume, it hits gas mixture atoms or molecules and ionizes them. The whole chamber is held in an uniform electric field, which is responsible for drift of

electrons resulting from ionization in the direction of readout pads. The electrons are multiplied on several wire planes and finally clusters are created on the pad plane. Then the signal is read by the electronics of readout plane.

The drift volume is covered with electrodes forming the electric field inside. They are made of aluminized Mylar strips of 25μm thickness and 0.5 inch width. They are close to the chamber walls and arranged perpendicular to the drift direction. The voltage applied to the electrodes is gradually decreased with the distance from the readout plane to about -19 kV in MTPCs and -13 kV in VTPCs. The voltage on the Mylar strips is applied using a resistor voltage divider chain.

In the upper part of the TPCs, near the readout pads, there is a MWPC (MultiWire Proportional Chamber). It consist of a plane of very thin (20μm) wires in close proximity, which makes a density of electric field very high close to them. Electrons while approaching the wires gain energy which allows them to further ionize gas molecules and atoms. The process called gas amplification creates an avalanche of 10^3-10^6 electrons from each electron from primary ionization. This results in clusters covering 3-4 pads on the readout plane.

There is also a plane of gating wires, called the gating grid. It is used to select appropriate events. The gate is open only during charge collection from the drift volume. In order to prevent unwanted events or debris from the drift volume from entering the readout region, the wires are polarized alternatingly with positive and negative voltage of $\pm$50V. To open the gate one has to apply the same voltage to all the wires. It is open only for 50μs in each event, so the drift velocity should be chosen very precisely in order to read tracks even from the bottom of the drift velocity. Closing the gate between events prevents unnecessary gas amplification which could cause ageing effects on the wires.

The readout pads are the most important elements of the TPC detector. Each detector is divided into sectors and each sector has its own multiwire chamber. Sectors are subdivided into padrows and padrows consist of pads. The shape of the pads is rectangular or trapezoidal and is optimized to minimize the angle between the track and the pad which is important for determining the cluster position. The detailed description of the pads is the following:

- **VTPC-1** All pads are 3.5 mm wide in the direction perpendicular to the beam. Pads in the sectors closest to the target (1 and 4) are 16 mm long and pads in other sectors are 28 mm long. The tilt angle is adjusted individually for each pad depending on its position from the beam and target,

	VTPC-1	VTPC-2	MTPC-L/R	GAP-TPC
Size[cm]	$250 \times 200 \times 98$	$250 \times 200 \times 98$	$390 \times 390 \times 180$	$30 \times 81.5 \times 70$
No. of pads/TPC	26886	27648	63360	672
Pad size[mm]	$3.5 \times 28(16)$	3.5×28	3.6×40,5.5×40	4×28
Drift length[cm]	66.60	66.60	111.74	58.97
Drift velocity[cm/μs]	1.4	1.4	2.3	1.3
Drift field[V/cm]	195	195	170	173
Drift voltage[kV]	13	13	19	10.2
Gas mixture	Ar/CO_2(90/10)	Ar/CO_2(90/10)	Ar/CO_2(95/5)	Ar/CO_2(90/10)
# of sectors	2×3	2×3	5×5	1
# of padrows	72	72	90	7
# of pads/padrow	192	192	192,128	96

TABLE 1.2: Parameters of TPCs

- **VTPC-2** All pads are 3.5 mm wide and 28 mm long. The tilt angle is increasing linearly with the distance from the beamline,
- **MTPC-L/R** All pads are 40 mm long. The five sectors closest to the beamline (21-25 in MTPC-L and 1-5 in MTPC-R) are called high resolution. The pads are 3.6 mm wide and are not tilted. The next five sectors (16-20 in MTPC-L and 6-10 in MTPC-R) are called standard resolution. They are 5.5 mm wide and are not tilted. The remaining sectors (1-15 in MTPC-L and 11-25 in MTPC-R) are called standard resolution prime. They are 5.5 mm wide and are tilted by an angle of 15°

The total number of pads in the five TPCs is 181926 (not including the LMPD). A single readout from a pad is called a timeslice. The time of a single readout is 50μs and 256 timeslices make up each event. Signal from the pad is read by 8-bit ADC. This results in over 44MB of data from each event. Position of a cluster on x and z direction provides us with information about track position in two dimensions. Because electrons after primary ionization drift with a constant velocity, we can calculate precise position of a track in three dimensions. It is done using precise time of flight detection. A single time slice corresponds to 2.6mm in VTPCs and 4.4mm in MTPCs. Usually the detected signal covers a few pads in one padrow and a few timeslices. This is called a cluster. Calculating the mean x and y position of a cluster allows for a better resolution.

1.2.4 Time of Flight detectors

There are two main Time of Flight detectors in the NA61/SHINE, ToF-L and ToF-R. They are scintillator detectors and are used to measure the arrival time of particles with a precision of 60ps. The measurement of particle velocity is obtained by dividing the distance from the interaction point by the time between beam detection and particle arrival to ToF detector. Knowing the velocity and momentum, we can calculate the

particle mass from the relativistic formula

$$p = \frac{\beta}{\sqrt{a-\beta^2}}mc \Rightarrow m^2 = \left(\frac{p}{c}\right)^2\left(\frac{1}{\beta^2}-1\right) = \left(\frac{p}{c}\right)^2\left(\frac{c^2t^2}{s^2}-1\right)$$

where p is the particle momentum, c - the velocity of light, m the mass of the particle, $\beta - \frac{v}{c}$, s - length of flight and t - measured time of flight. Used together with TPCs, ToF can improve the precision of particle identification.

1.2.5 Projectile Spectator Detector

The PSD (Projectile Spectator Detector) is a calorimeter used for precise measurement of the projectile spectator energy in nucleus-nucleus collisions. It is used for the selection of central collisions at the trigger level. Only events with a small number of projectile spectators are chosen. The PSD allows also for precise event-by-event measurements of the energy carried by projectile spectators enabling the extraction of the number of interacting nucleons from the projectile with the precision of one nucleon. The high energy resolution of the PSD is important for the study of fluctuations in nucleus-nucleus collisions which are expected to be sensitive to properties of the phase transition between quark-gluon plasma and hadron-resonance matter. The PSD provides precise control over fluctuations caused by the variation of the number of interacting nucleons and thus exclude the fluctuations caused by variation of the collision geometry.

The PSD consists of 44 modules of different sizes. There are 16 smaller modules with a transverse dimensions of $10 \times 10\text{cm}^2$. They are located on the beamline to decrease the spectator occupancy in one module and improve the reconstruction of the reaction plane. The outer part of the PSD consist of 28 larger modules, each of them $20 \times 20\text{cm}^2$ in transverse plane. Each module consists of 60 pairs of alternating lead plates and scintillator layers with 16mm and 4mm thickness, respectively. The particle going through the detector looses its momentum and energy in the lead layers and we can determine its initial energy measuring which scintillator did the particle achieve before it stopped.

Chapter 2

Time Projection Chambers calibration

2.1 Krypton calibration idea

The main objective of Time Projection Chambers in the NA61/SHINE experiment is particle identification using the dE/dx method. In order to achieve precise dE/dx measurements it is crucial to have information about the detector response (pads gain). The gain is specific for each pad and consists of a gas gain and electronics response fluctuations.

The idea of the method is to inject the radioactive $^{83}_{36}$Kr isotope into TPCs. The decay spectrum of $^{83}_{36}$Kr is very well known, therefore we can use it for the purpose of calibration by comparing the response of the electronics in the different pads. Having large enough statistics (a sufficient number of radioactive decays registered by the readout electronics) it is possible to create a high granularity map of gains. This allows us to:

- Precise study of gas gain and readout electronics fluctuations,
- Calibration of the above,
- Cross-check with different calibration methods.

The method has been developed by the ALEPH collaboration, but nowadays it is commonly used in other experiments adapting TPCs, i.e. ALICE.

The description in following sections is largely based on [3].

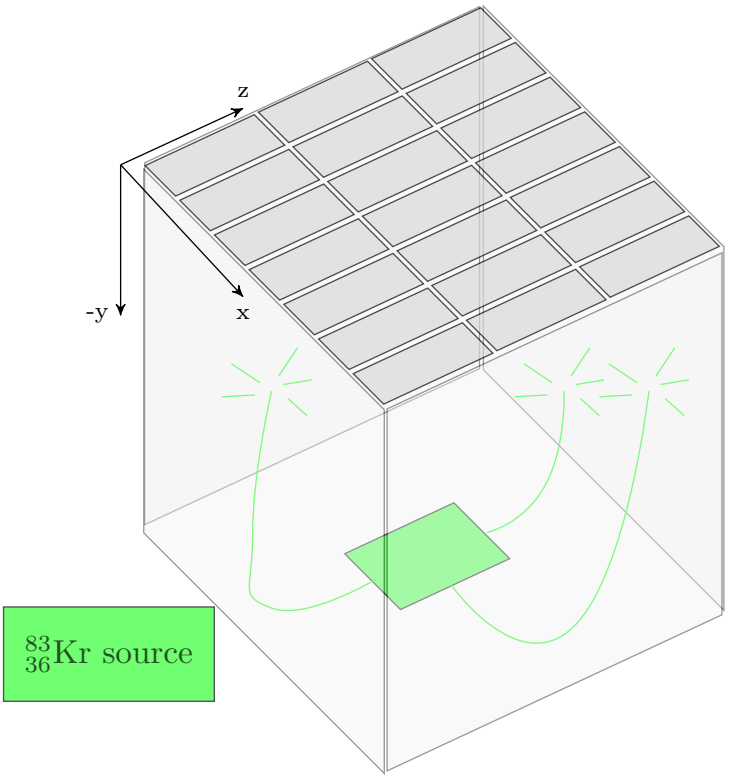

FIGURE 2.1: Schematic view of krypton source in TPC with decay points

2.2 Krypton calibration scheme

A sample of the radioactive $^{83}_{37}$Rb source is placed in the bypass of TPCs gas system. The radioactive krypton gas is being emitted from the source and slowly fills the volume of the TPCs. From its unstable state, it decays down and emits various radiation. The decay leaves a specific spectrum on the readout pads in form of energy deposit. The data is taken with a time trigger, because there is no beam incoming into TPCs. Due to differences in gain on the readout pads, the registered spectrum is scaled on different pads. The scaling occurs only on the x axis. If the gain is higher, the spectrum is wider and vice versa. The relative gain can be obtained by comparing position of the peaks on the resulting spectra.

The radioactive $^{83}_{36}$Kr krypton gas is obtained from the $^{83}_{37}$Rb source by electron capture. After the reaction it is mostly in an unstable state of 41.6 keV excitation energy with a half life of 1.9 hr. Deexcitation to the ground state passes through an intermediate state of 9.4 keV with a short half life of 147 ns. Therefore we have two nuclear decays with 32.2 and 9.4 keV transition energy.

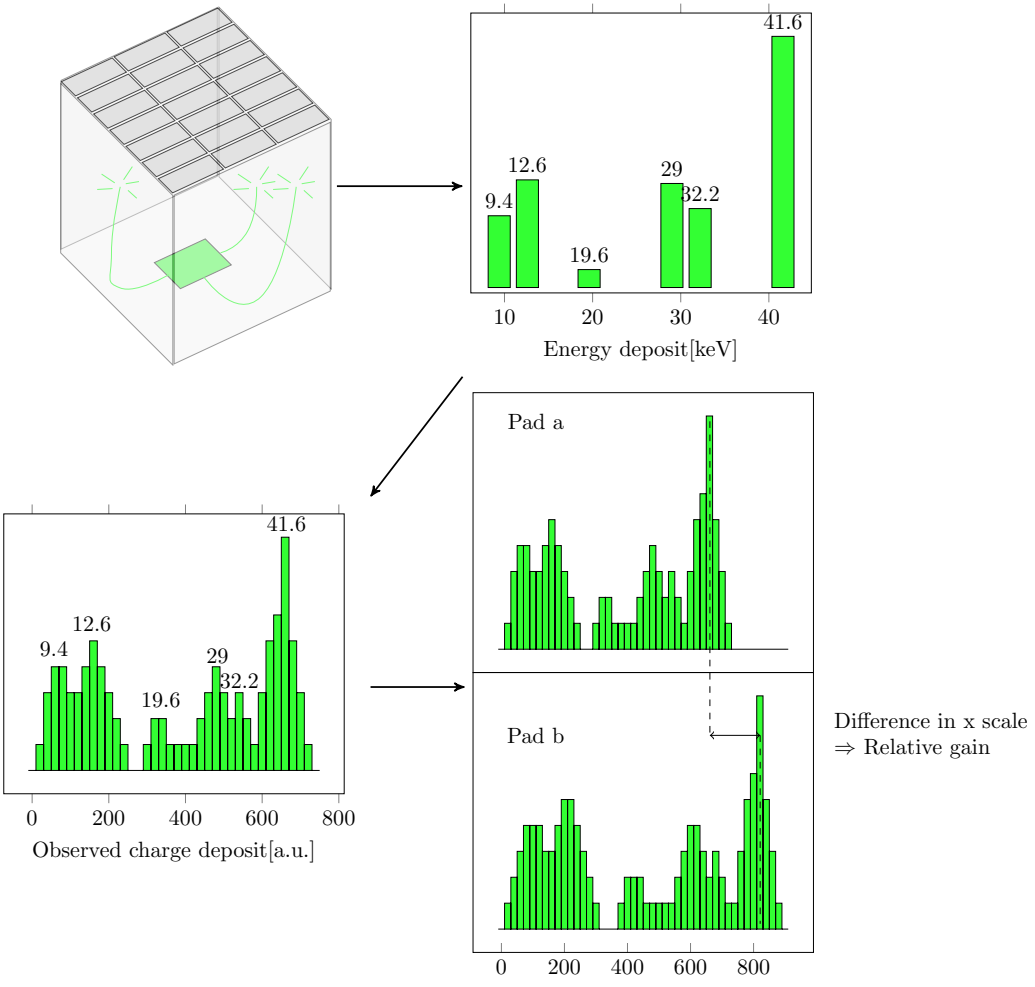

FIGURE 2.2: An overview of the Kr calibration method

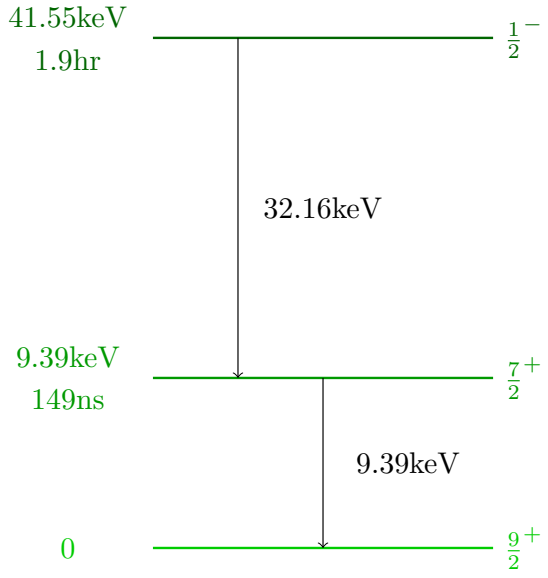

FIGURE 2.3: Diagram of deexcitation of $^{83}_{36}$Kr

2.3 Physics of krypton decay

The 32.2 keV transition is almost entirely dominated by IC (internal conversion) which is followed by atomic deexcitations - X-ray photon emission and Auger transition. This process results in a number of electrons with well defined energies not exceeding 32.2 keV plus possibly one X-ray photon with energy between 12.6 and 14.3 keV.

The 9.4 keV transition is also dominated by IC, but with a relative probability of 4.9% a 9.4 keV gamma emission is also observed. The subsequent atomic deexcitations are Auger transitions. Once again, the final outcome are electrons with a given energy and possibly one photon with 9.4 keV energy.

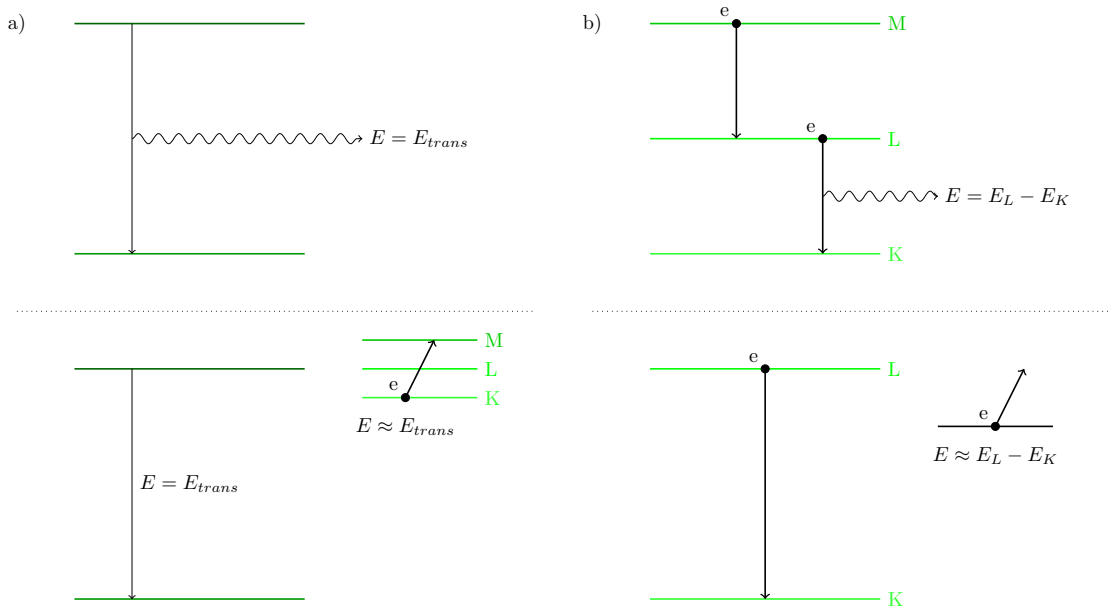

FIGURE 2.4: Schematic illustration of the two nuclear decays
a) The nuclear transition proceeds either through direct gamma emission from the nucleus (upper panel) or through internal conversion - nuclear transition energy E_tran is transmitted to an electron of lower atomic shell
b) The atomic deexcitation: atomic shells emptied by internal conversion are filled with electrons from higher levels. The energies difference is emitted through X-ray and by Auger emission.

Following facts about the nature of the detector and the gas mixture should be remembered:

- Photons emitted in the transitions can interact with the gas molecules via the photo-electric effect. The radiation length is of an order of 30 cm, which gives us free electrons in the volume,

- All the free electrons present in the volume (IC, Auger or photo-electric effect) ionize gas molecules. Because the electron energy is relatively low, the resulting ionization tracks are short (below 2 cm),
- Electrons coming from Auger and IC transitions are emitted directly at the decay point, which will result in a single electron cluster on the TPC readout electronics. A separate cluster will appear as a result of each of the photon emissions,
- The half life of the intermediate state is so short (147 ns) that two electron clusters appearing on the electronics can in fact be regarded as a single cluster.

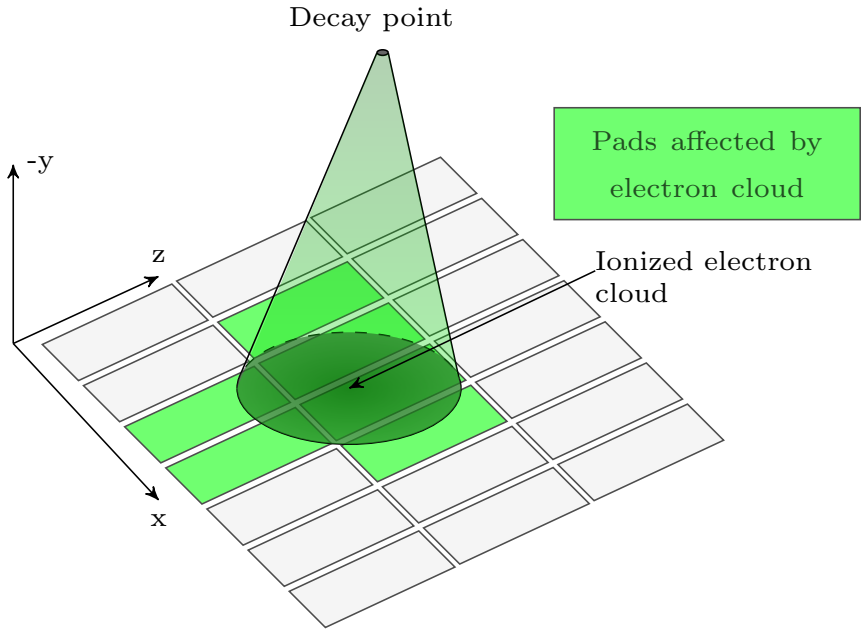

FIGURE 2.5: Schematic view of a krypton cluster

Summing up, the deexcitation of the $^{83}_{36}$Kr isotope can have the following effects on the readout electronics:

- a single electron cluster in the decay point, corresponding to an energy deposit of up to 41.6 keV,
- one or two more electron clusters resulting from photon emission, located at a large distance (of an order of 30 cm) from the decay point with energy deposit varying between 9.4 and 14.3 keV.

Effectively, we obtain a characteristic spectrum of energy deposit, illustrated in 2.6. Although peaks have now a sizable width, most of them are well distinguishable.

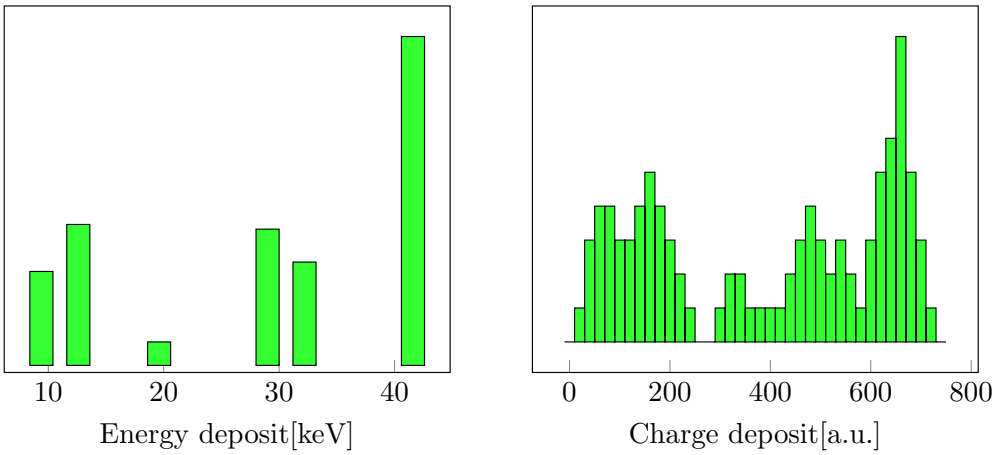

FIGURE 2.6: **a)** Energy deposit spectrum resulting from $^{83}_{36}$Kr decay. **b)** Charge deposit spectrum with basic detector effects

2.4 Different calibration schemes

Pulser calibration, which can also be used for cross-checking Kr calibration is described in Appendix A.

Chapter 3

Krypton calibration scheme

Krypton calibration of Time Projection Chambers consists of the following steps:

1. Krypton data taking - radioactive $^{83}_{36}$Kr gas from $^{83}_{37}$Rb source is injected into the Time Projection Chambers. Readout electronics on each pad detect $^{83}_{36}$Kr decays and save information about measured signals,
2. Krypton data reading - reading krypton events from raw files done by EventFileReader included in the SHINE framework,
3. Finding clusters - an algorithm chooses only clusters of readout pads satisfying ADC value threshold,
4. Readout of cluster properties - data read by cluster finder and its properties is saved into the root format,
5. Cuts on clusters - removal of clusters which are certainly created by malfunctioning electronics,
6. Estimating peak position - in a region which is free of noise, we analyze total Kr spectrum to find approximate position of the peak,
7. Integral check - an algorithm checks if a charge spectrum from Kr decays does not come from noise,
8. Peak finding - an algorithm finds the main peak in the krypton spectrum, which is easily distinguishable. Then it saves the peak position for each pad,
9. Calculating gain - using the main peak position we can obtain gain factors for each pad.

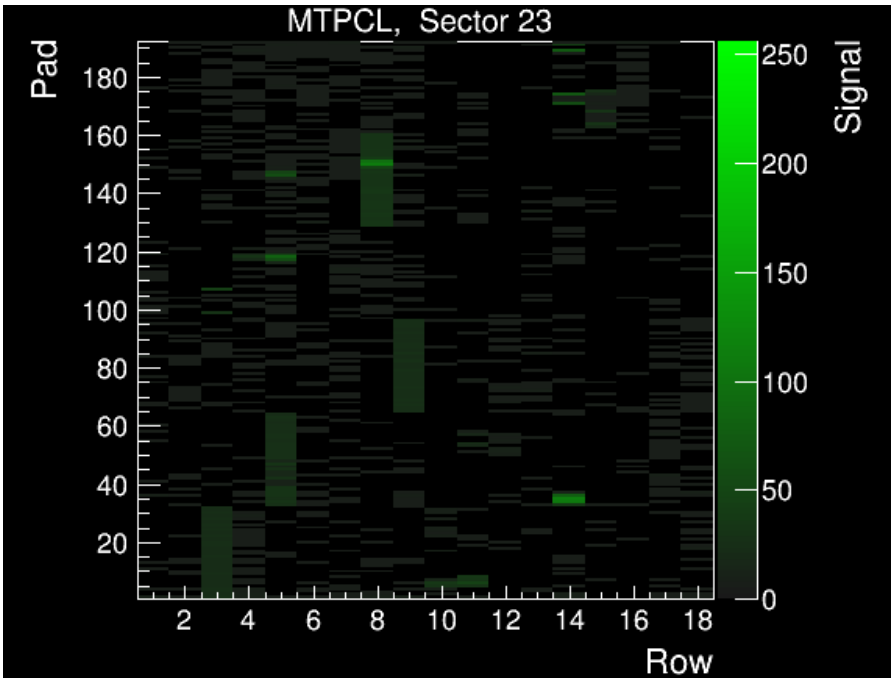

FIGURE 3.1: Overview of signal strength received by sector 23 of MTPCL. There is a Kr cluster visible in padrow number 14, between pads 33 and 38.

The charge accumulated on the readout pads gets converted by FEE (Front End Electronics) into the digital form. The readout takes place in consecutive short time intervals. Because there is no beam used in krypton runs, intervals are triggered in constant time separation by a global clock. 256 time slices with 200 ns time bins are used. First, the analog signal is stored in capacitor arrays and later it is digitized via a Wilkinson ADC(Analog to Digital Converter).

3.1 Cluster finder

The cluster finding procedure was developed by Andras Laszlo. It is used to find contiguous islands of high ADC signal on each padrow. The procedure is invoked if an ADC value on a given pad is higher than the threshold value (it is currently set to 9 ADC, which corresponds to ~ 3 sigma).

Once the procedure is initiated, we check the pad's neighbors if their ADC passes the threshold of 6 ADC (corresponding to ~ 2 sigma of noise). In case they do, we add pads to the clusters and look for this criterion also in its neighboring ADCs. The procedure is presented as a block diagram on drawing 3.4. A physical overview of the procedure is shown on drawing 3.3.

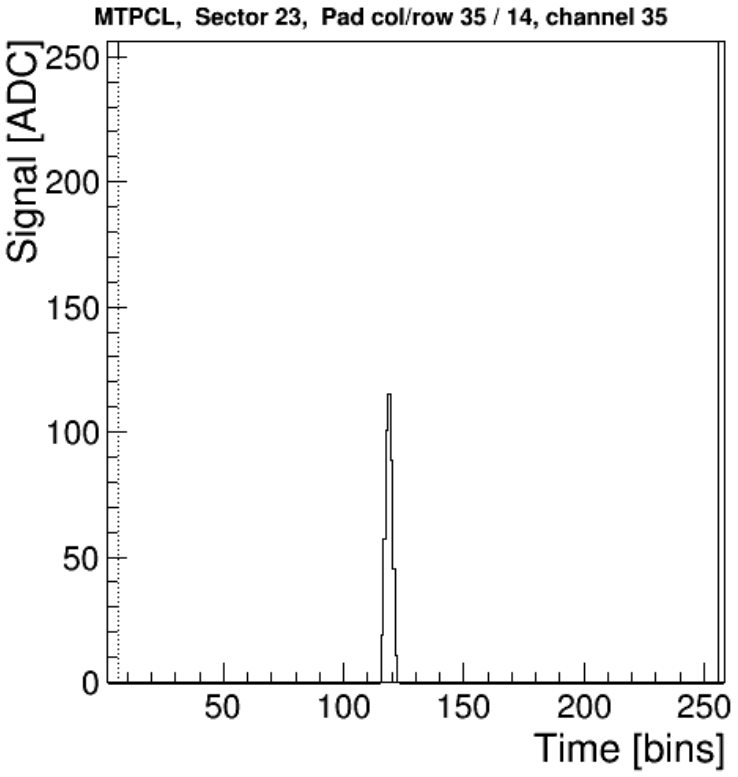

FIGURE 3.2: Overview of signal received by single pad.

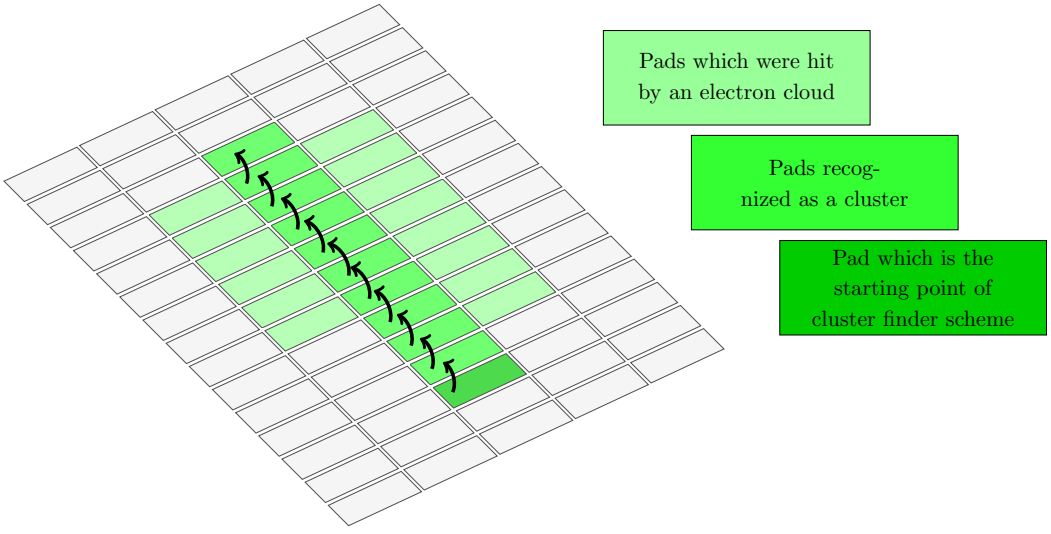

FIGURE 3.3: Presentation of the cluster finding scheme on the readout plane

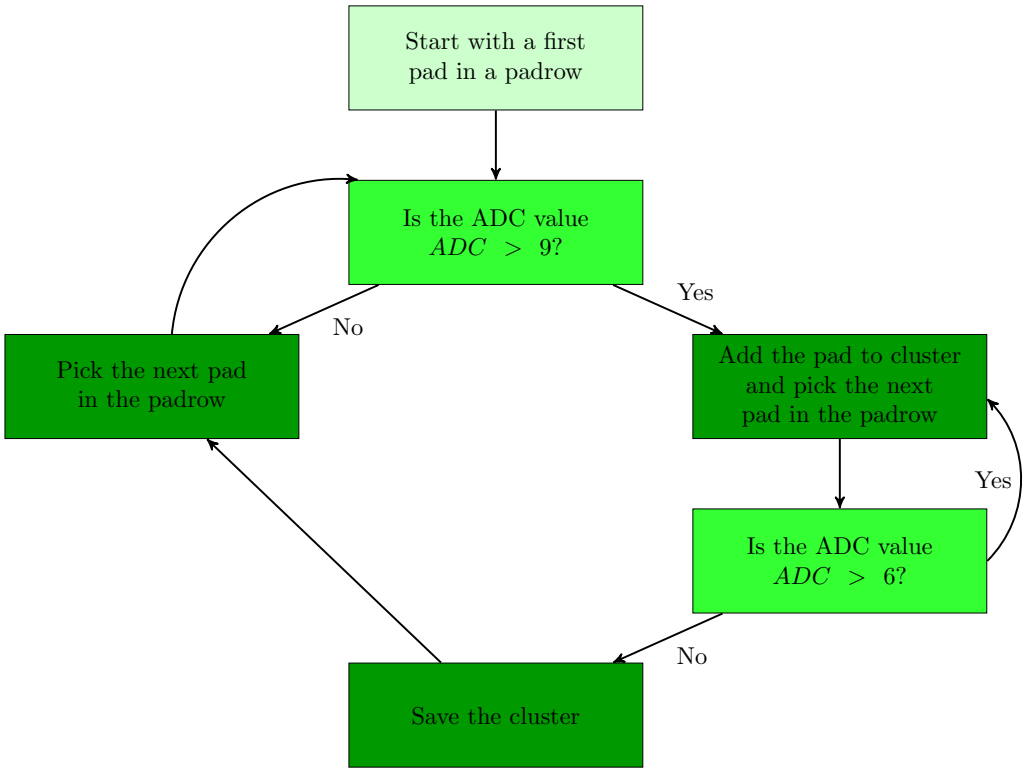

FIGURE 3.4: Presentation of the cluster finding algorithm. All steps are repeated until the end of the padrow.

3.2 Readout of cluster properties

When the cluster finder accepts a given cluster, it saves information about its properties. In the next step, properties valuable for krypton calibration are saved into a root file in form of a root TTree. Characteristics of a cluster that are being saved are presented in table 3.1.

The charge value is an integrated charge from cluster's pads and maximum ADC value refers to a maximum ADC value contained in a single pad in this cluster. Y position usually describes the vertical position of a particle track. As there is no trigger in krypton calibration, the Y position value is sometimes used to remove noises coming from gating grids of TPCs. Number of pads, timeslices and pixels describe the cluster span of pads, timeslices and $2D(numberOfPads \times numberOfTimeslices)$ pixels, respectively.

3.3 Cuts on clusters

In order to roughly remove from our analysis data that definitely comes from electronics noise or malfunctioning pads, cuts on given properties of clusters are introduced. We

Value	Data type	Name
Charge	/F	charge
Maximum ADC	/b	maxADC
Y coordinate	/D	yCoordinate
Number of pixels	/s	numberOfPixels
Number of timeslices	/s	numberOfTimeslices
Number of pads	/b	numberOfPads
TPC ID	/s	TPC
Sector number	/b	sector
Padrow number	/b	padrow
Pad number	/b	pad

TABLE 3.1: Nodes saved in a root TTree. Data types are following:

- /F a 32 bit floating point (Float_t)
- /D a 64 bit floating point (Double_t)
- /s a 16 bit signed integer (Short_t)
- /b an 8 bit unsigned integer (UChar_t)

expect Kr clusters to be small in terms of number of timelsices and pads (and therefore pixels) because of physical properties described earlier. Since one FEE readout chip is connected to 16 pads we can consider clusters containing 16 or more pads as produced by malfunctioning chips. We should also limit the number of timeslices. The cuts I introduce are following:

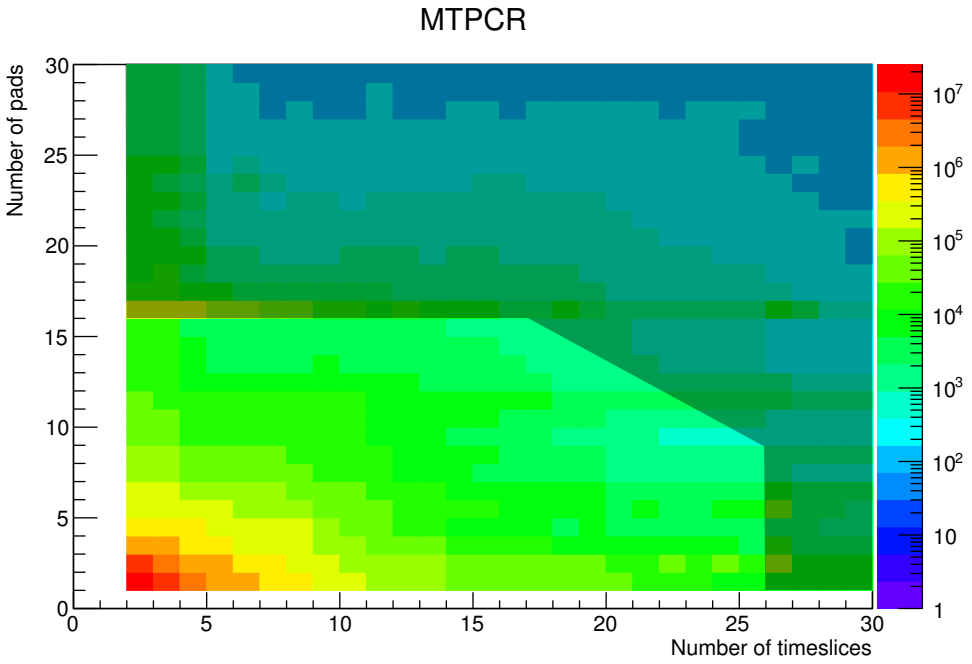

FIGURE 3.5: Presentation of introduced cuts. The clusters in the darkened part of histogram are refused.

$$
\begin{aligned}
numberOfPads &< (numberOfTimeSlices - 30) * -2/3 \\
numberOfTimeSlices &< 22 \\
numberOfPads &< 16
\end{aligned}
$$

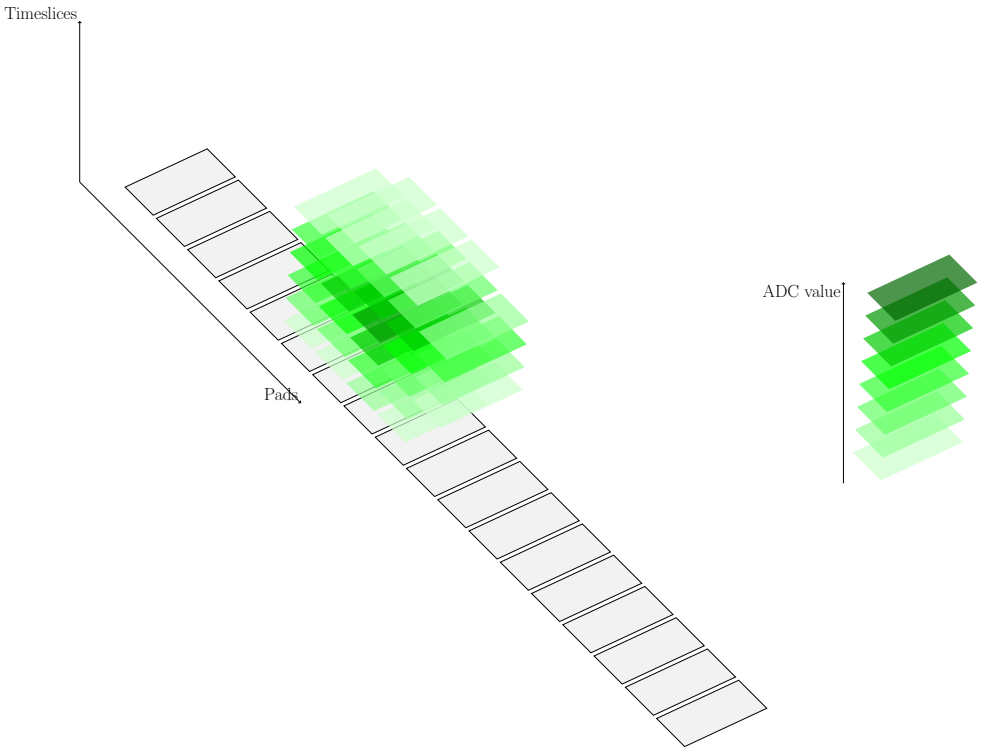

FIGURE 3.6: Figure presenting a cluster which would be accepted according to introduced cuts

The above cut is a safe solution, as it only removes $\sim 10\%$ of clusters found by cluster finder.

3.4 Estimating peak position

Each of the time projection chambers presents a different characteristic of the received Kr spectrum. In MTPC-L and MTPC-R differences between high and low resolution sectors are expected. In VTPC, sectors 1 and 4 have different geometry and can also present different spectrum characteristics. The main difference is the position of the main peak in spectrum. Depending on the region of the TPC, its position will be in different total charge values.

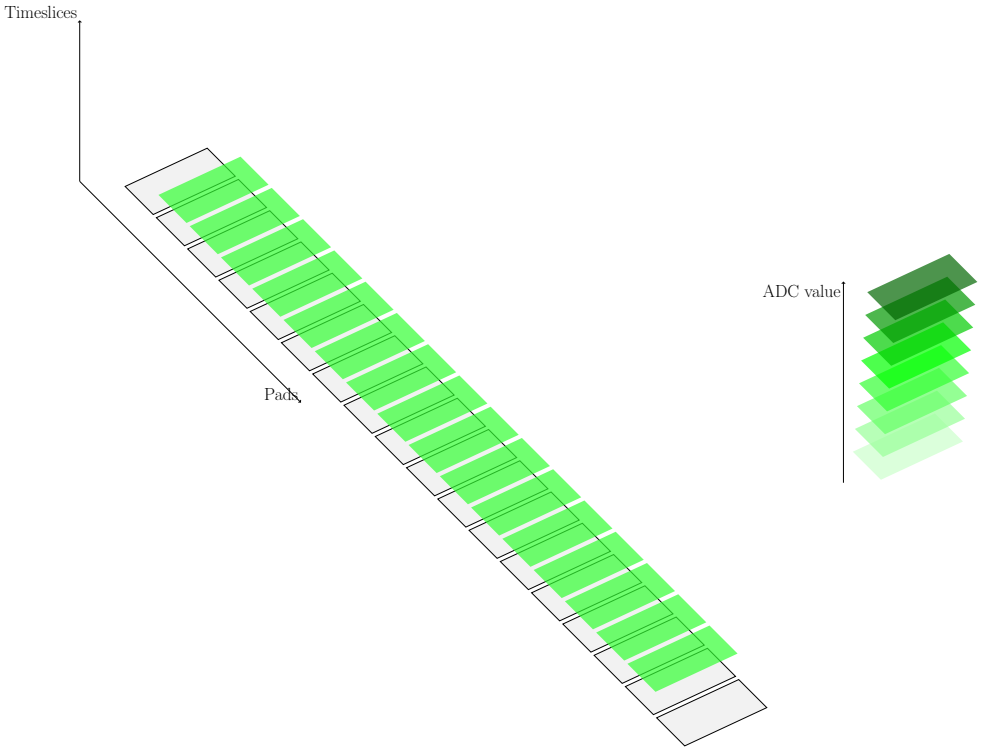

FIGURE 3.7: Figure presenting a cluster which would be rejected, because the number of pads is higher than 15. It might come from a malfunctioning chip, as the number of pads in cluster is equal to 16

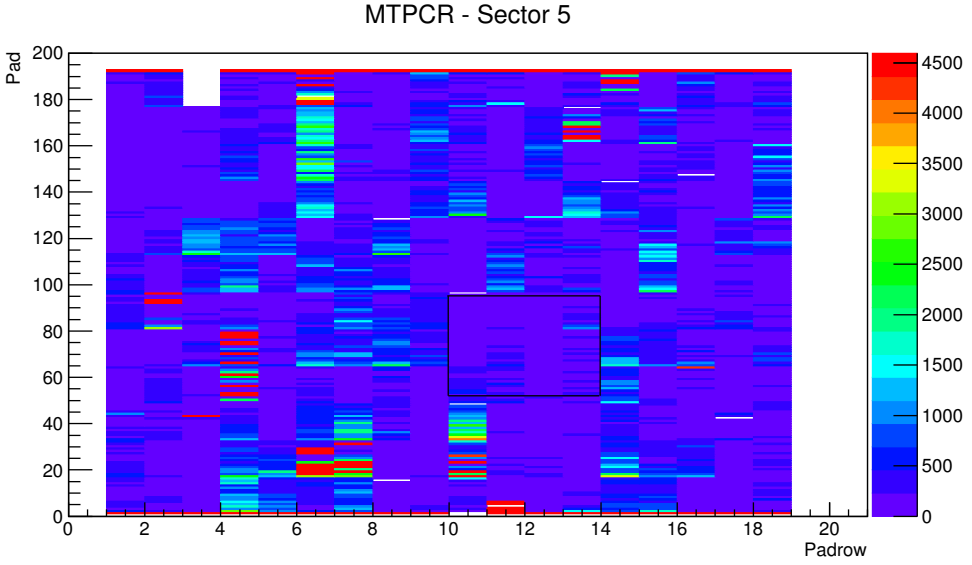

FIGURE 3.8: An overview of a uniform region in MTPC-R

A simple way of determining the approximate peak position in a given region has been developed. On the histogram of a number of clusters found on the pad plane for the region we look for places with uniform distribution of the number as shown on figure 3.8. For the places we draw the total Kr spectrum summing over all pads. Then we can roughly determine the peak position. The procedure is presented on figure 3.9

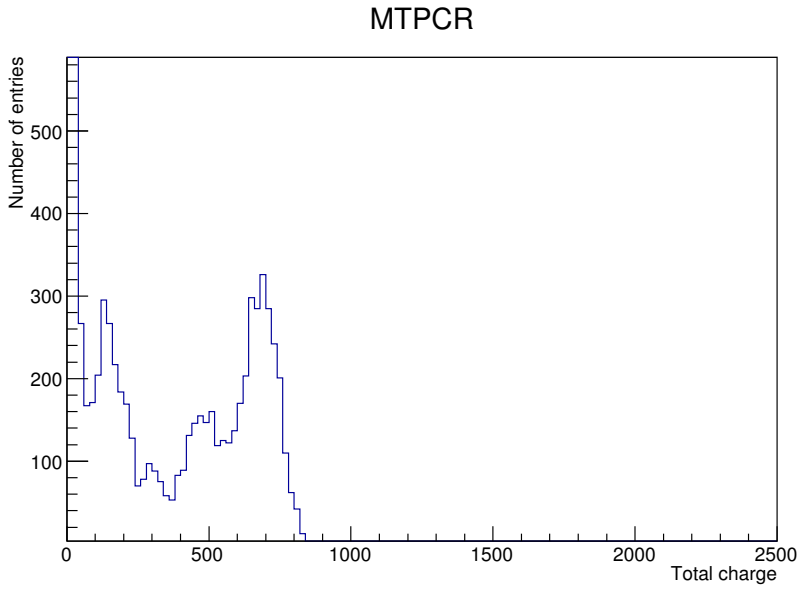

FIGURE 3.9: Total Kr spectrum for the uniform region. The main peak position is approximated to be $Q \in (500, 1000)$

3.5 Integral check

Detailed analysis of the Kr spectrum in GTPC leads to a conclusion about the nature of noise received by pads. GTPC was chosen for analysis because of reasonable number of pads being equal to 672. It allowed for a deep analysis of the Kr spectrum coming from every pad. The study resulted in the finding that in pads which are considered noisy there is an unreasonably high number of clusters (of an 10^3 order of magnitude) for very low total charges. These peaks can not be associated with any of the ${}^{83}_{36}\mathrm{Kr}$ decays.

Using this fact we can create a simple way of detecting pads infected with noise of the latter nature. Pads affected by noise should manifest much higher integral under the Kr spectrum for low total charges than for higher charges. Comparing the integrals in two regions $(0; Q_{\mathrm{end}})$ and $(Q_{\mathrm{start}}; Q_{\mathrm{end}})$, where Q_{start} and Q_{end} are respectively the beginning and the end of the area where the peak is expected to occur, will allow to decide if the pad should be rejected or not.

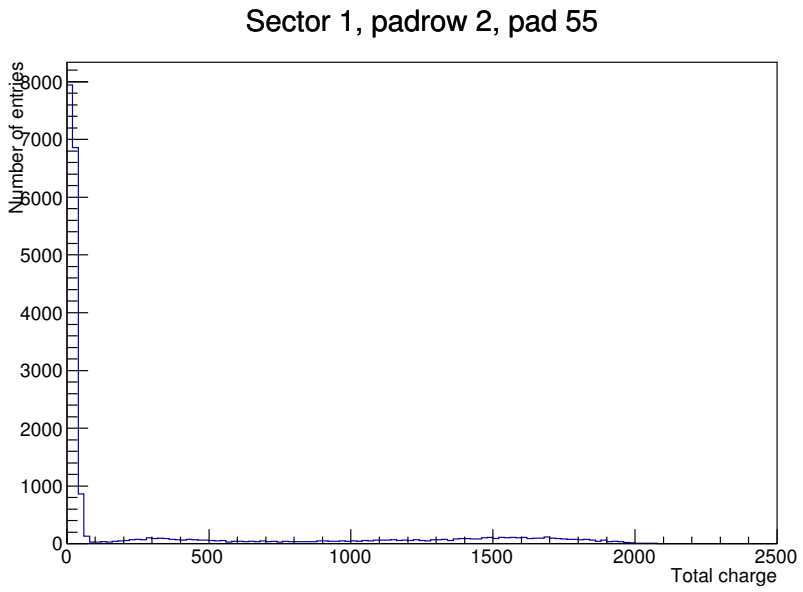

FIGURE 3.10: Example of a GTPC pad affected by noise. Characteristic unreasonably high peak for low charges is clearly visible

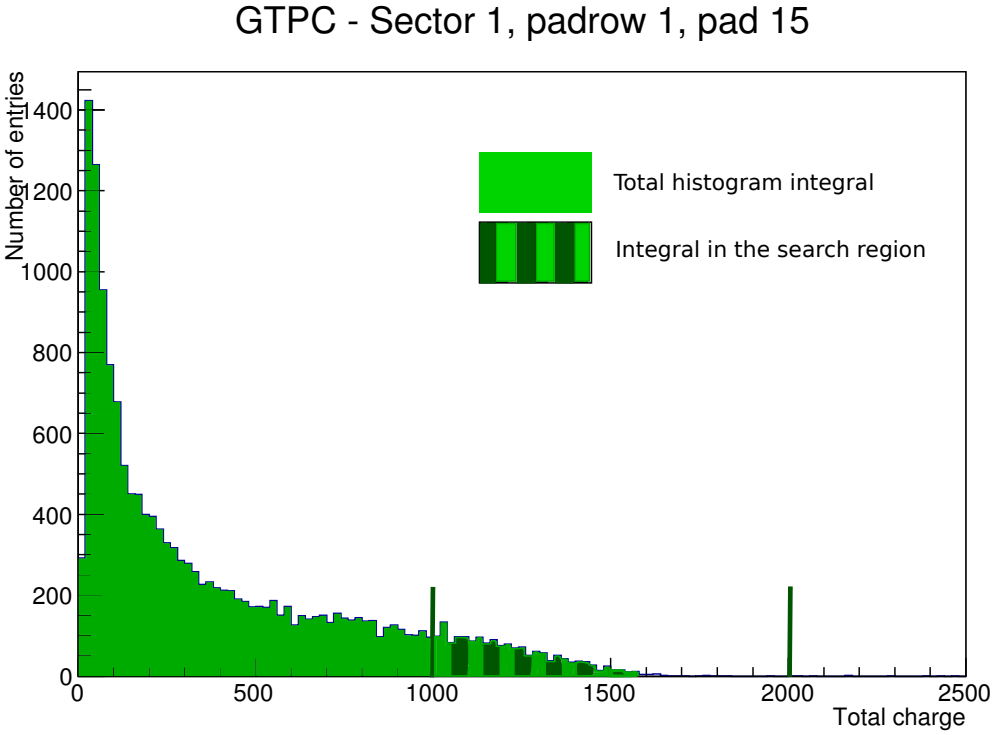

FIGURE 3.11: Overview of the integral check method

Therefore I reject pads which satisfy the following condition:

$$A_{\text{total}} > \alpha A_{(Q_{\text{start}};Q_{\text{end}})}$$

where the factor α is expect to be small, around 5. The factor can be precisely determined utilizing the next calibration step. The number of pads rejected by peak finder is strongly dependent on the α parameter. For α higher or equal to threshold value β, the number of pads rejected suddenly grows. Consequently one can chose

$$\alpha = \beta - 1$$

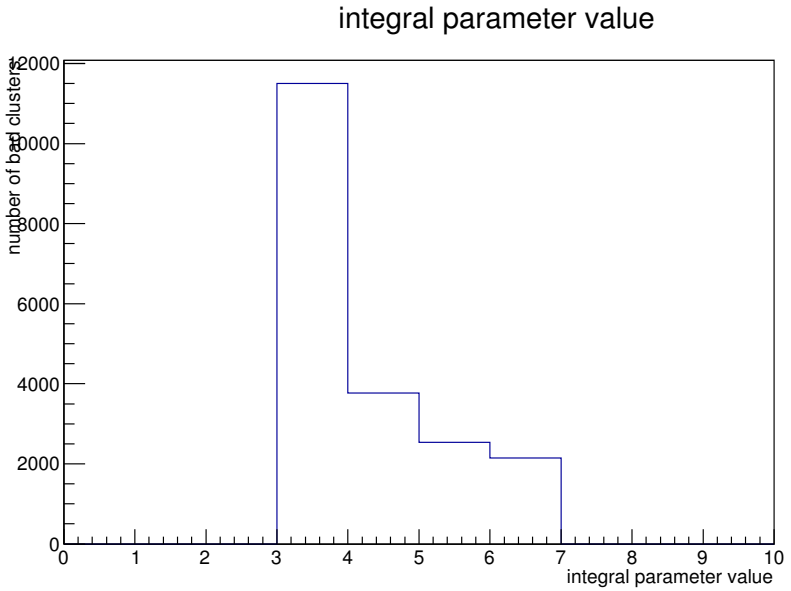

FIGURE 3.12: Dependence of the number of rejected pads on the α parameter

I also reject pads which have no spectrum at all, which means that they are not working

$$A_{\text{total}} = 0$$

3.6 Peak finding

The peak finding algorithm is the most important and the most demanding part of the Kr calibration process. It utilizes all the information obtained in previous steps, i.e. approximate peak position, rejected pads and cuts on clusters. The result of the peak finder is a map of pads with gains associated with them. An overview of the peak finding process is presented on figure 3.13.

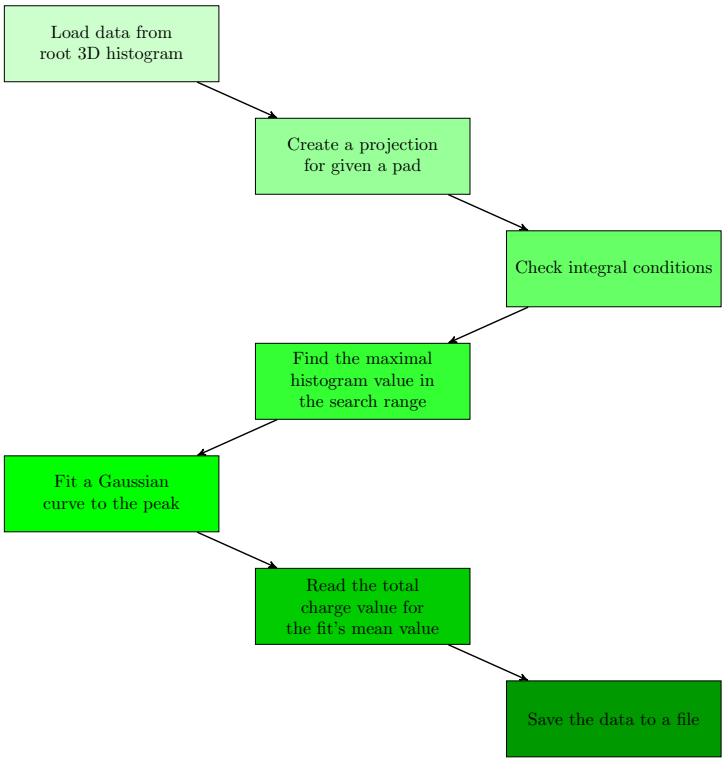

FIGURE 3.13: An overview of the peak finding procedure

The data that is used in this step is held in form of separate root 3D histograms for every sector of the TPCs. One dimension is occupied by number of padrow, second by number of pad and third by total charge. Therefore we have all the Kr spectra for a given sector in one file. In order to extract the data one has to use the root ProjectionX method that allows to project a 3D histogram into a one dimensional histogram for a given x and y axis range. In this case we want to extract just one pad histogram, so we have to project on a specific pad and padrow number.

Finding the maximal value of the histogram is a complicated task as GetMaxBin method in root does not allow to limit the search region to a predefined approximate peak position Q. Therefore, one has to create a copy of histogram with nonzero values only in the search region. Then using GetMaxBin method returns appropriate result q.

In order to fit a Gaussian curve to the main Kr peak I use the Fit method of the TH1D histogram. I provide a standard root Gaussian function with L argument, which uses the loglikelihood penalty function. The loglikelihood penalty function is more appropriate in the case of Kr peaks as they are tall and narrow. The search is only limited to a close region around the maximal histogram value $q \pm 70$. If the peak is not found, the pad is marked as malfunctioning.

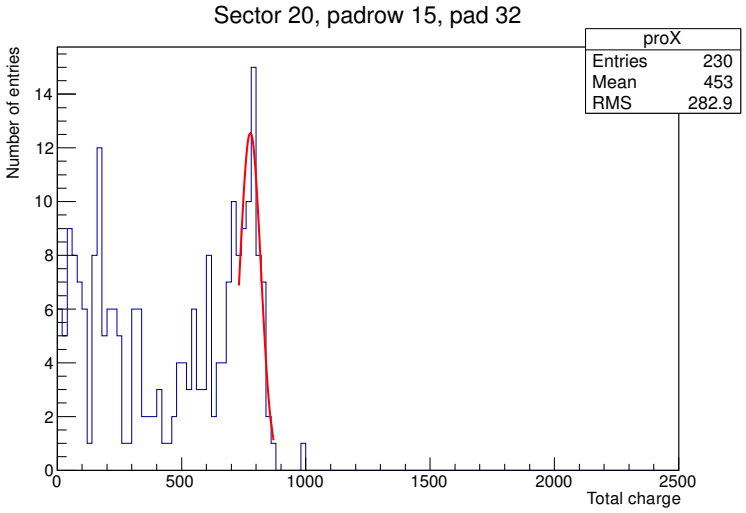

FIGURE 3.14: An example of Gaussian fitting

As a last step we save the position of the Gaussian fit maximum on the total charge axis. For the purpose of Kr calibration the relative gain factors are necessary. To obtain them, one needs to know a pad that is for sure working correctly and its peak position q_{corr}. We have to find such pads for all the TPCs. Then it is easy to calculate the gain factor

$$G_i = \frac{q_i}{q_{\text{corr}}}$$

For the purpose of this thesis we will only consider Kr peak positions, not gain factors.

Chapter 4

Results

The results of Kr calibration will be presented in this chapter. For each time projection chamber there will be a separate section containing information regarding all steps of calibration described in chapter 3. The final result will be presented in form of a map of all pads with the corresponding main peak position.

For the purpose of calibration data taken during the September 2014 run was utilized. Details of data used are presented in the table 4.1

Detector	Run number	Number of chunks	Number of clusters	Total size	HV (HR)[V]	HV (SR)[V]
VTPC 1	18348	32	$3.5 \cdot 10^6$	67 GB	1100	1070
VTPC 2	18374	18	$6.5 \cdot 10^6$	37 GB		900
GTPC	19201	2	$7.9 \cdot 10^6$	2.4 GB		
MTPC-L	18298	60	$6.9 \cdot 10^6$	122 GB	920	980
MTPC-R	18248	60	$8.9 \cdot 10^6$	122 GB	890	960

TABLE 4.1: Details of data used for Kr calibration

An overview of parameters used for the calibration process is presented in table 4.2

Detector	Q_{start}	Q_{end}	α	Number of malfunctioning pads
VTPC 1	800	2200	4	3900
VTPC 2	800	1700	4	7305
GTPC	500	2500	4	7
MTPC-L LR	700	1500	4	9116
MTPC-L HR	800	1800	4	1603
MTPC-R LR	500	1200	3	9808
MTPC-R HR	400	1100	3	3096

TABLE 4.2: Parameters used for Kr calibration

4.1 VTPC1

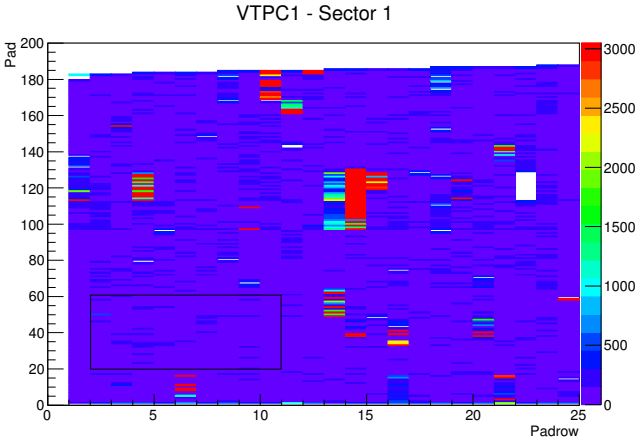

FIGURE 4.1: Overview of the VTPC1 Sector 1. The uniform area of histogram is marked with the black rectangle

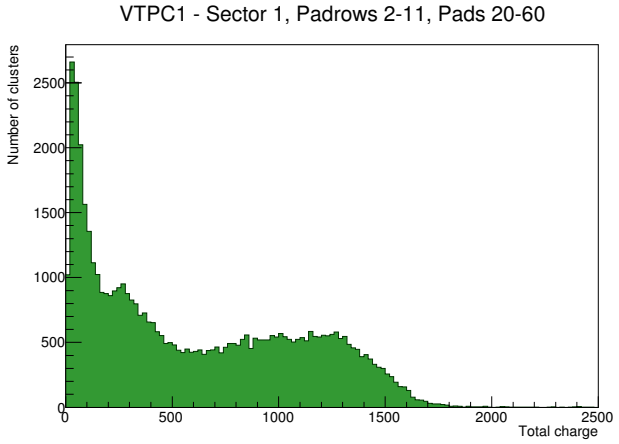

FIGURE 4.2: Total charge from the selected region. The peak position is estimated to be in $(800, 2200)$ region

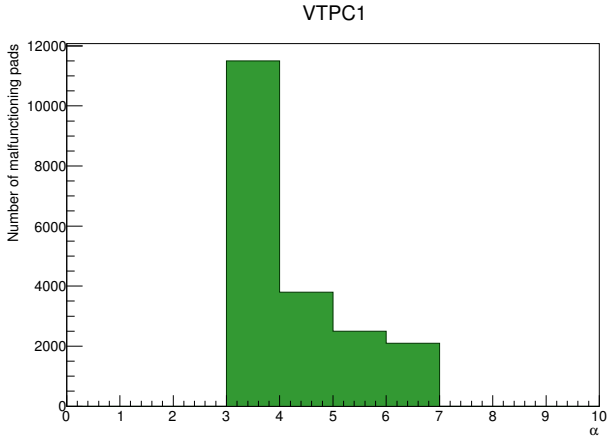

FIGURE 4.3: Plot of the integral parameter α value and number of malfunctioning pads found. From this plot we estimate $\alpha = 4$

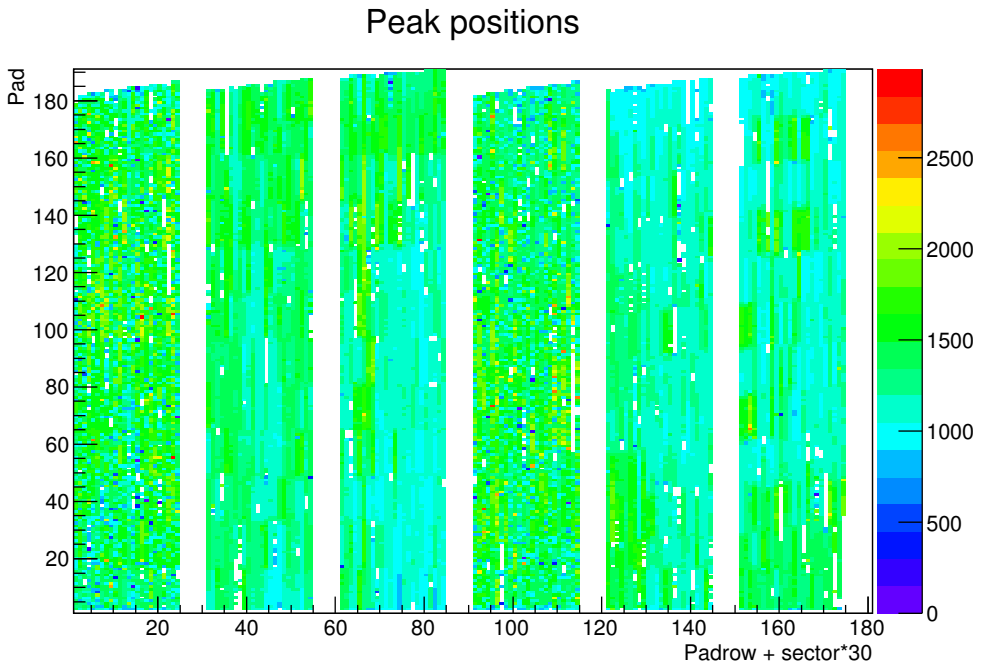

FIGURE 4.4: Map of the main peak position for each pad in VTPC1

4.2 VTPC2

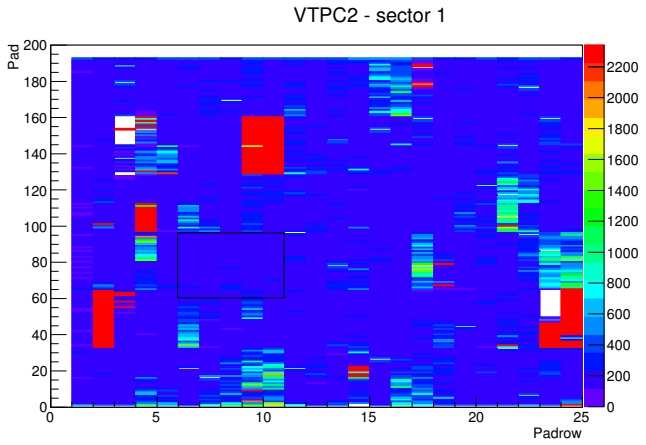

FIGURE 4.5: Overview of the VTPC2 Sector 1. The uniform area of histogram is marked with the black rectangle

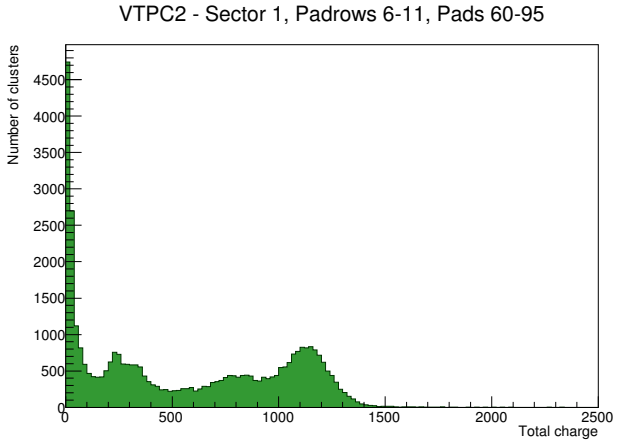

FIGURE 4.6: Total charge from the selected region. The peak position is estimated to be in $(800, 1700)$ region

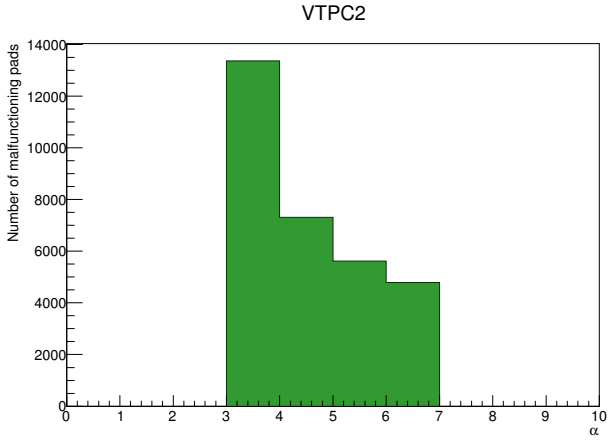

FIGURE 4.7: Plot of the integral parameter α value and number of malfunctioning pads found. From this plot we estimate $\alpha = 4$

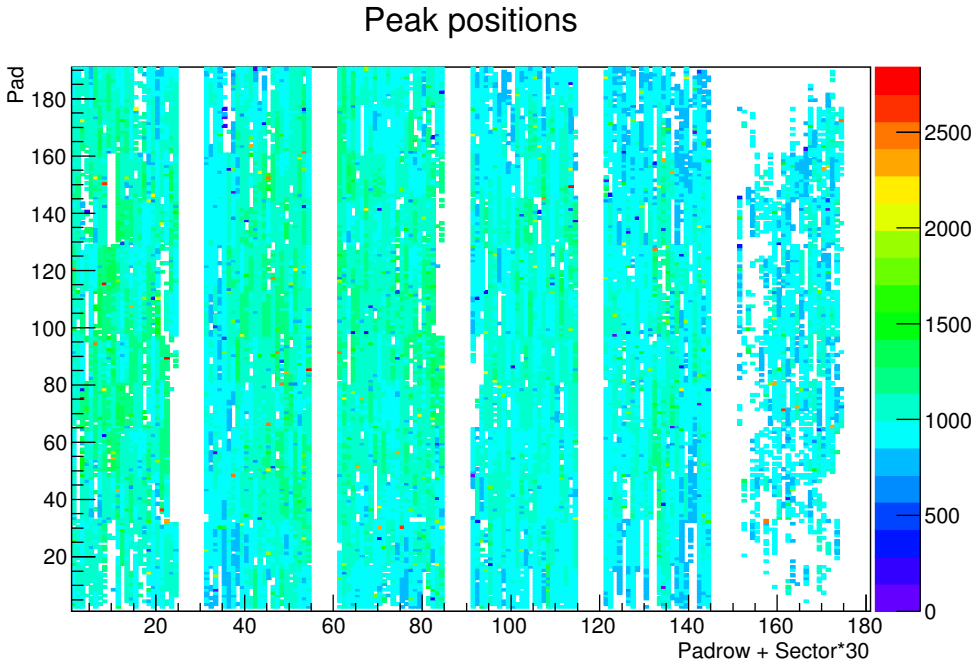

FIGURE 4.8: Map of the main peak position for each pad in VTPC2

4.3 GTPC

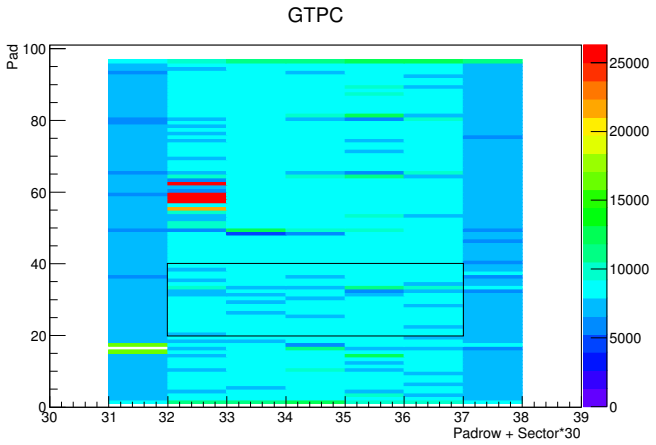

FIGURE 4.9: Overview of the GTPC Sector 1. The uniform area of histogram is marked with the black rectangle

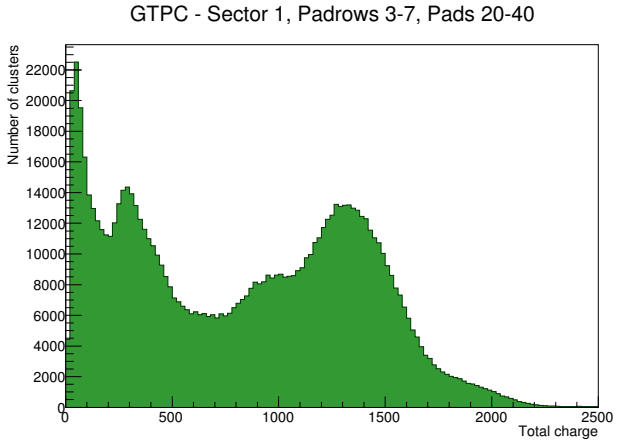

FIGURE 4.10: Total charge from the selected region. The peak position is estimated to be in $(500, 2500)$ region

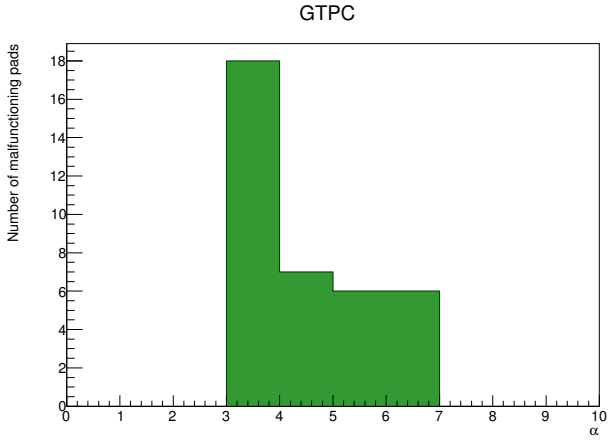

FIGURE 4.11: Plot of the integral parameter α value and number of malfunctioning pads found. From this plot we estimate $\alpha = 4$

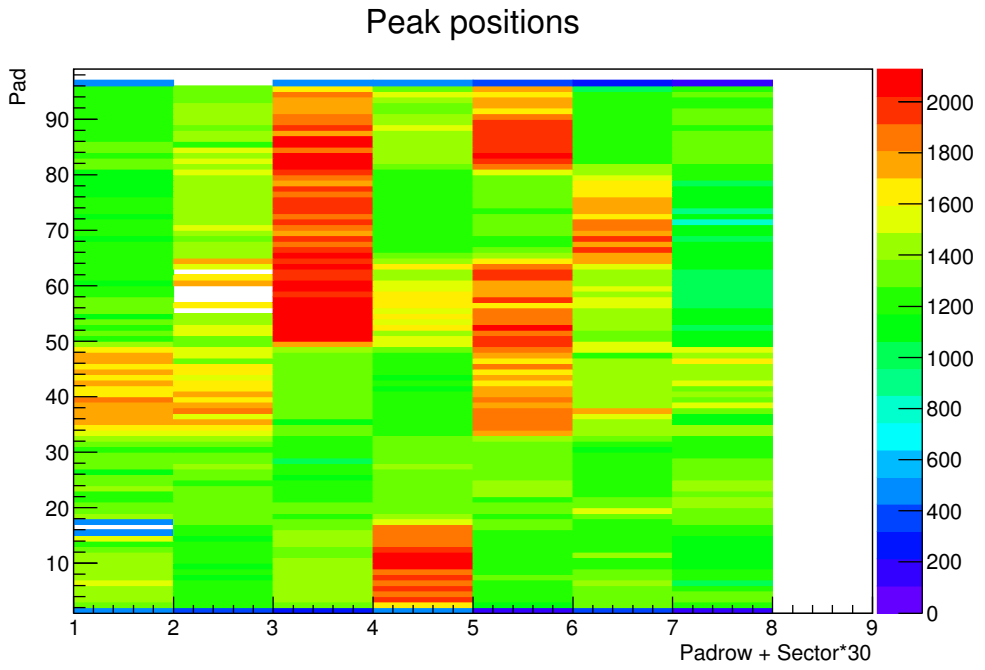

FIGURE 4.12: Map of the main peak position for each pad in GTPC

4.4 MTPC-L

4.4.1 High resolution pads

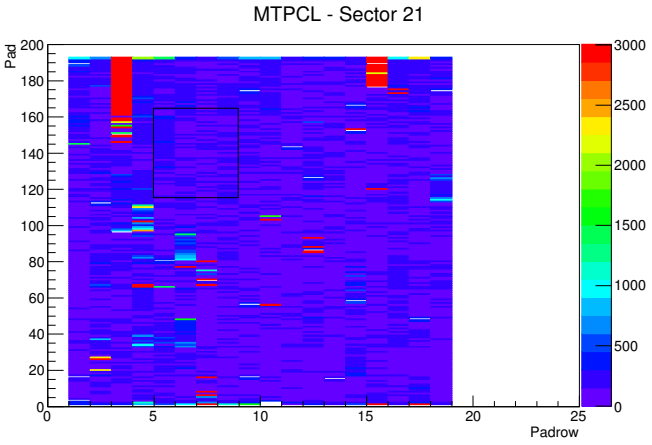

FIGURE 4.13: Overview of the MTPC-L Sector 21. The uniform area of histogram is marked with the black rectangle

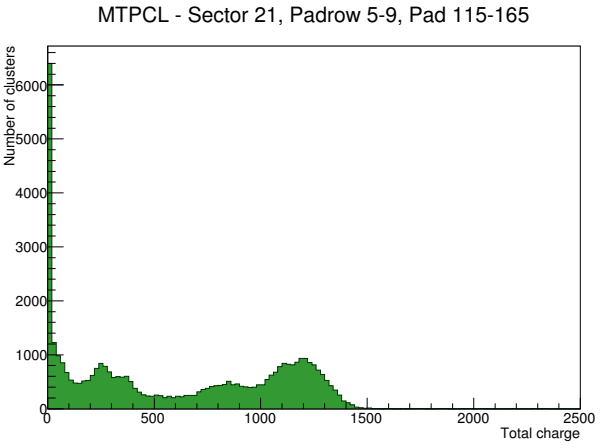

FIGURE 4.14: Total charge from the selected region. The peak position is estimated to be in $(800, 1800)$ region

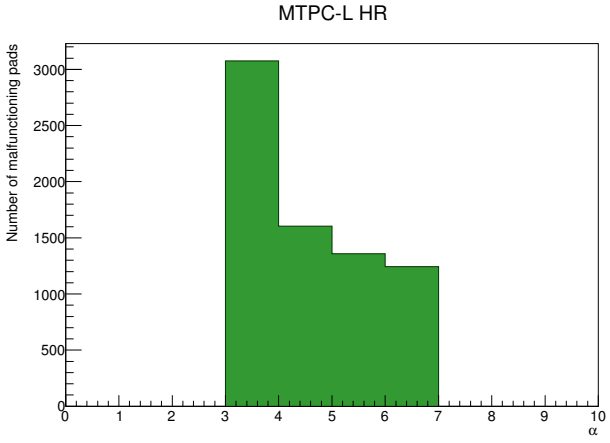

FIGURE 4.15: Plot of the integral parameter α value and number of malfunctioning pads found. From this plot we estimate $\alpha = 4$

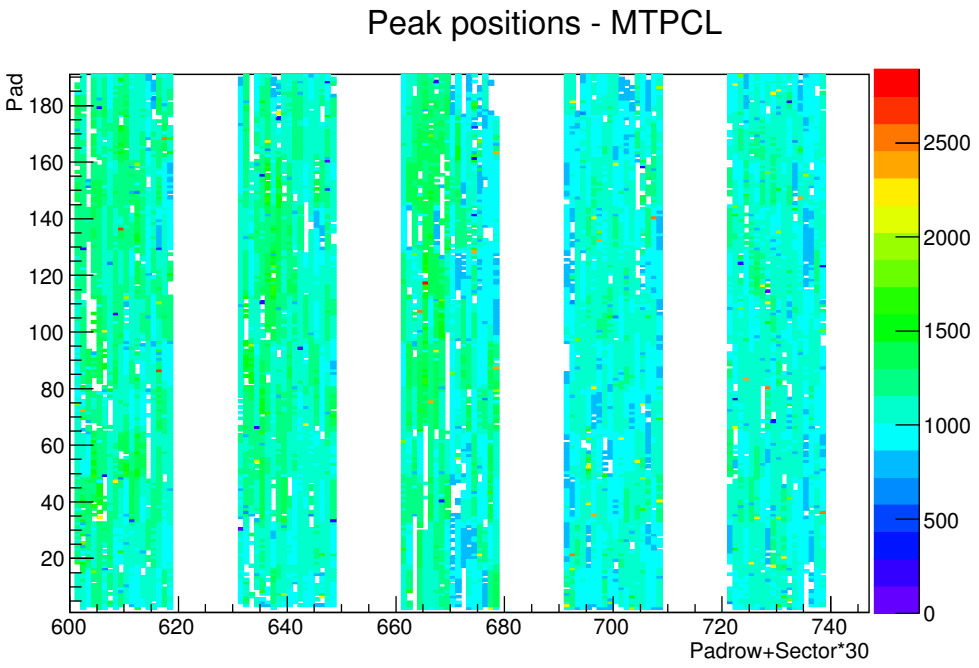

FIGURE 4.16: Map of the main peak position for each LR pad in MTPC-L pads

4.4.2 Low resolution pads

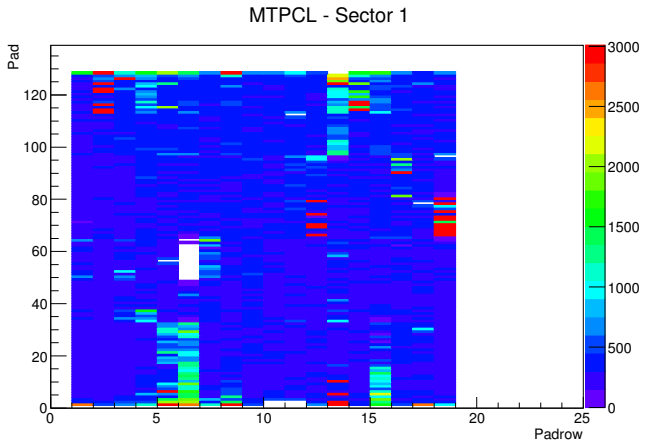

FIGURE 4.17: Overview of the MTPC-L Sector 1. The uniform area of histogram is marked with the black rectangle

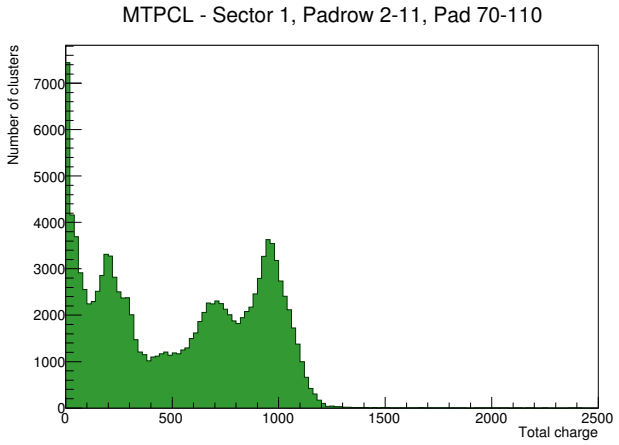

FIGURE 4.18: Total charge from the selected region. The peak position is estimated to be in $(700, 1500)$ region

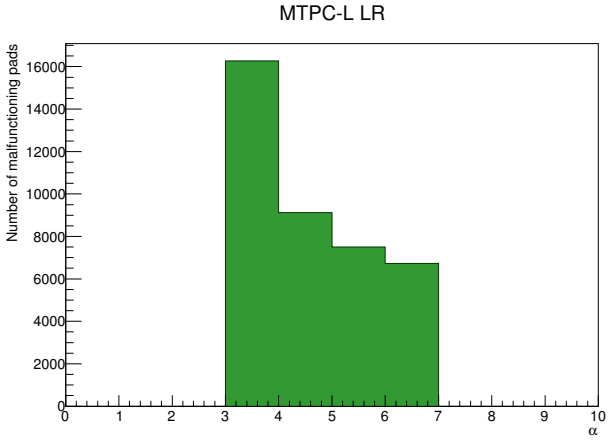

FIGURE 4.19: Plot of the integral parameter α value and number of malfunctioning pads found. From this plot we estimate $\alpha = 4$

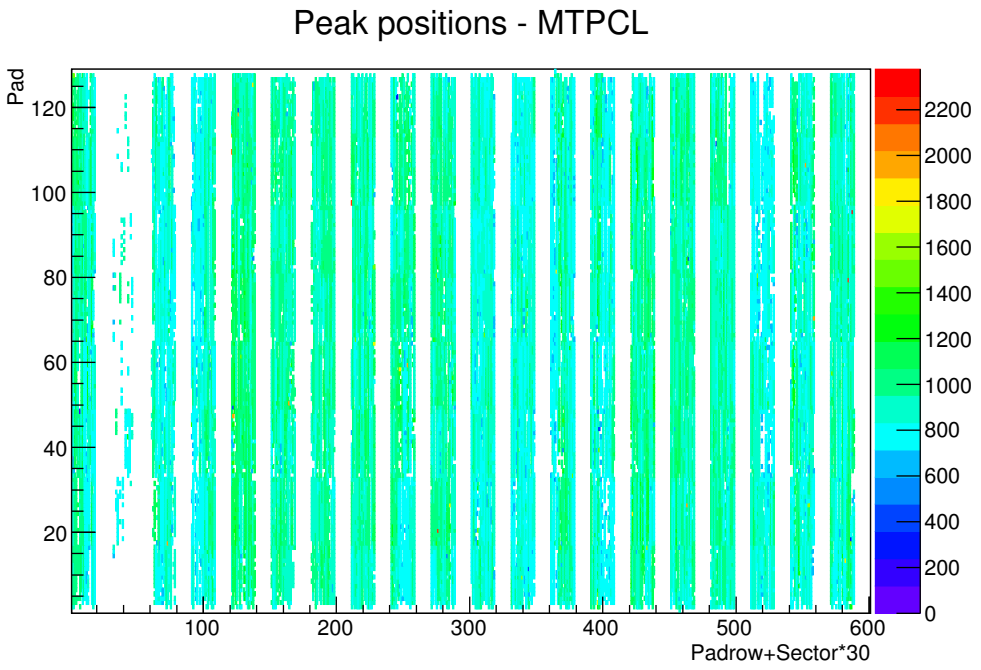

FIGURE 4.20: Map of the main peak position for each LR pad in MTPC-L pads

4.5 MTPC-R

4.5.1 High resolution pads

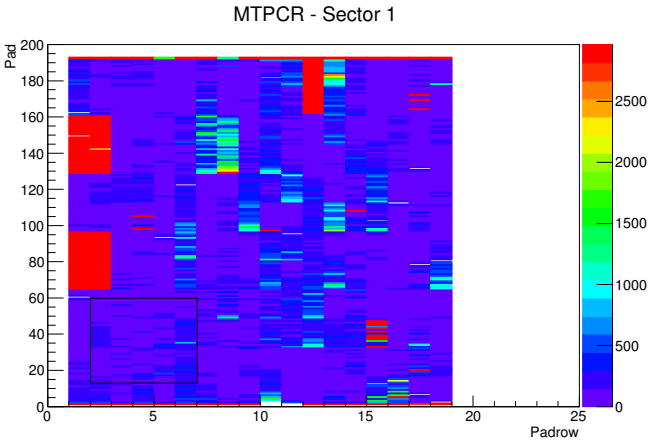

FIGURE 4.21: Overview of the MTPC-R Sector 1. The uniform area of histogram is marked with the black rectangle

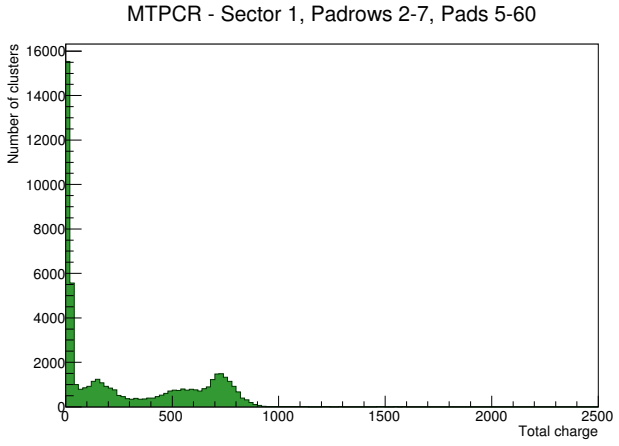

FIGURE 4.22: Total charge from the selected region. The peak position is estimated to be in $(400, 1100)$ region

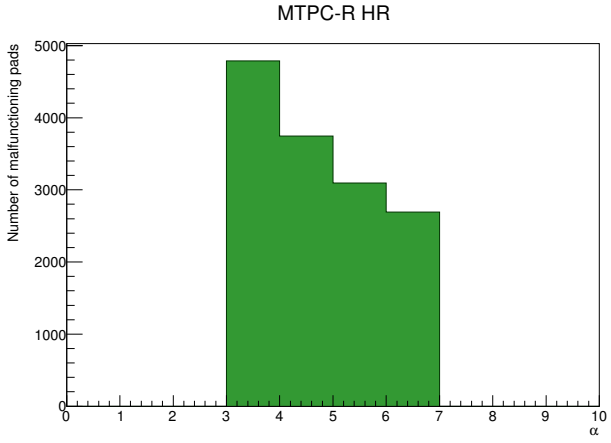

FIGURE 4.23: Plot of the integral parameter α value and number of malfunctioning pads found. From this plot we estimate $\alpha = 4$

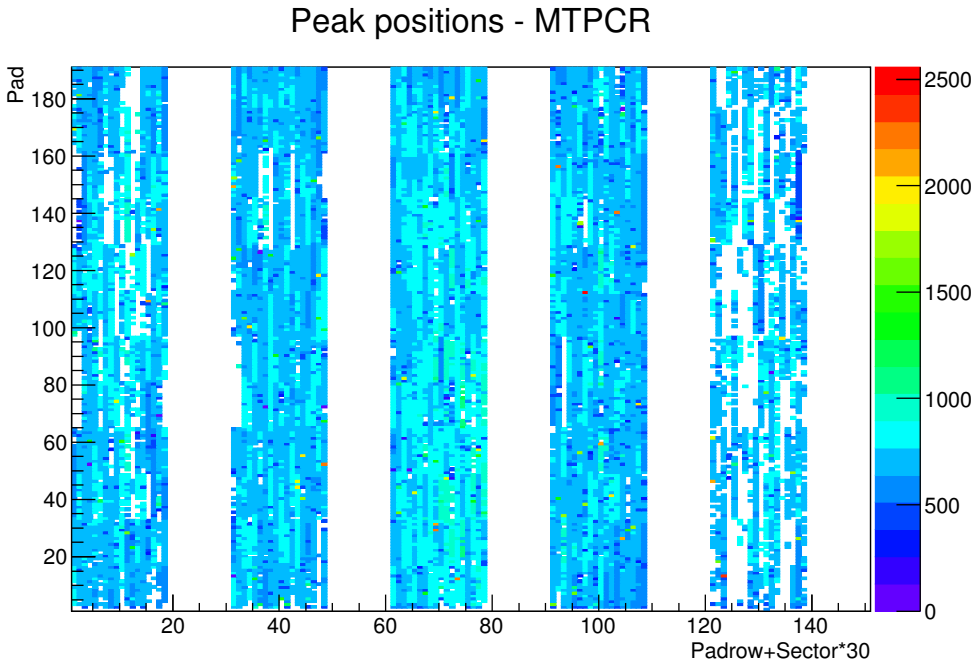

FIGURE 4.24: Map of the main peak position for each HR pad in MTPC-R

4.5.2 Low resolution pads

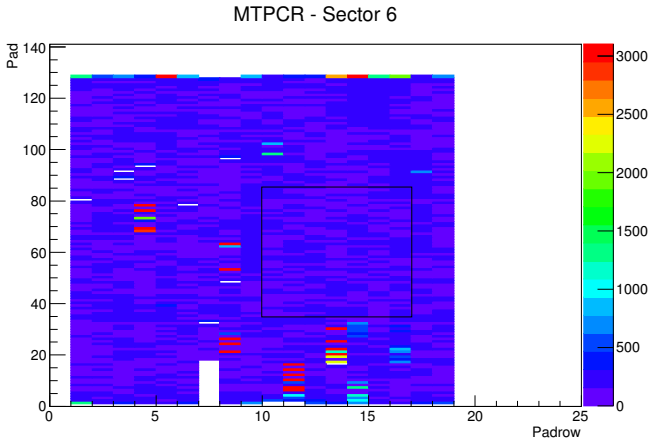

FIGURE 4.25: Overview of the MTPC-R Sector 6. The uniform area of histogram is marked with the black rectangle

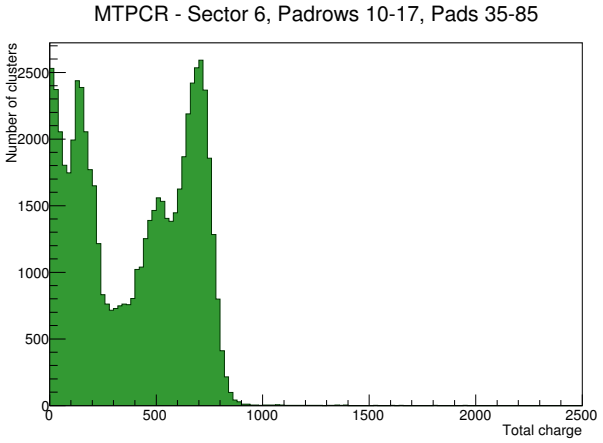

FIGURE 4.26: Total charge from the selected region. The peak position is estimated to be in $(500, 1200)$ region

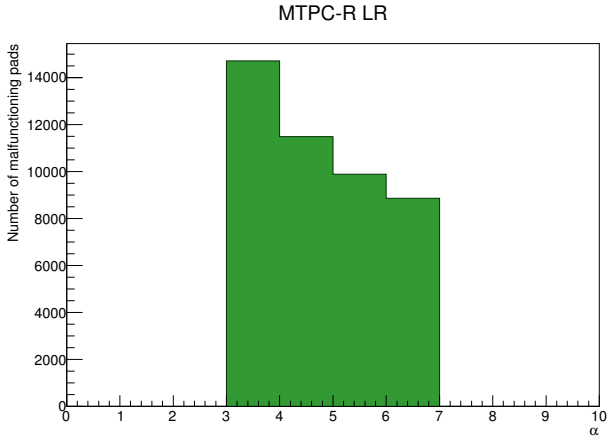

FIGURE 4.27: Plot of the integral parameter α value and number of malfunctioning pads found. From this plot we estimate $\alpha = 4$

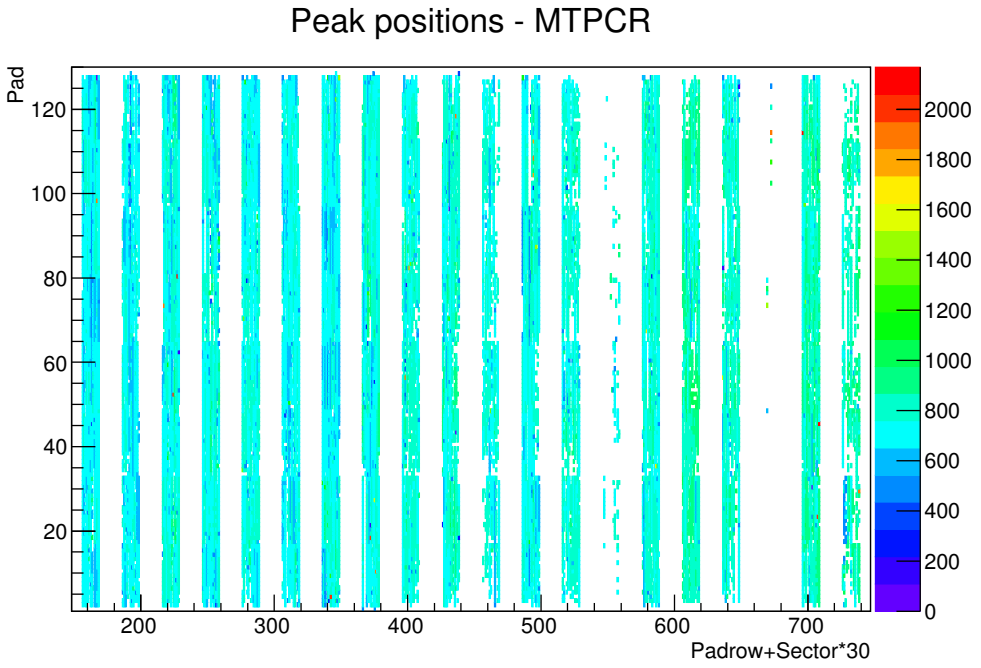

FIGURE 4.28: Map of the main peak position for each LR pad in MTPC-R

Chapter 5

Conclusions

5.1 Malfunctioning pads

One of the main tasks of krypton calibration is determining malfunctioning pads in the TPCs. This knowledge can significantly influence particle track reconstruction and its resolution. Malfunctioning pads may be caused by broken electronics and chips. This case should result in areas of malfunctioning pads in the same padrow. The size of such 'clusters' should be around 16 pads, as the same amount of pads is connected to one chip. Other possibility for corrupt pads is the process of aging. Since the TPCs were inherited from the NA49 experiment and are more then 20 years old, this process can be substantial for the number of malfunctioning pads.

Detector	№of pads	№of malfunctioning pads	Percentage of malfunctioning pads
VTPC 1	26886	3900	14%
VTPC 2	27648	7305	26%
GTPC	672	7	1%
MTPC-L LR	46080	9116	21%
MTPC-L HR	17280	1603	9%
MTPC-R LR	46080	9808	21%
MTPC-R HR	17280	3096	18%
Total	181926	34835	19%

Table 5.1: Percentage of broken pads in different TPCs

The Kr calibration process has not been carried out since the year 2010. Since then the percentage of malfunctioning pads might have substantially changed. The Kr calibration presented here is utilizing the most up to date data.

The number of broken pads differs from chamber to chamber. The relative number of the latter is the highest for the VTPC2, where almost half of the sixth sector is

producing noise. A similar situation can be found in the low resolution sectors of MTPC-L and MTPC-R. In both of the chambers there are sectors that have a majority of malfunctioning pads. These sectors are 19 and 23 in MTPC-R and 2 in MTPC-L. The situation is also present in the high resolution pads of MTPC-R and applies to sector 5. Otherwise the percentage of broken pads is rather homogeneous in all TPCs except GTPC, which is the youngest device.

This analysis implies that in order to increase the resolution of track reconstruction one should think first of repairing all of the malfunctioning sectors. This can give a significant decrease in the percentage of malfunctioning pads very quickly. Broken pads in other sectors might come from a regular aging process and are spread homogeneously in a similar amount.

5.2 Comparison with the pulser calibration

As described in appendix A, the pulser calibration can be used for cross check of the krypton calibration. In this section two methods will be compared on example of the GTPC. The krypton calibration is a complex operation, but resembles real processes happening in the chambers and therefore provides information about both - physical and electronic response of detector. Pulser calibration is only capable of measuring electronic response and can only be used for cross checks.

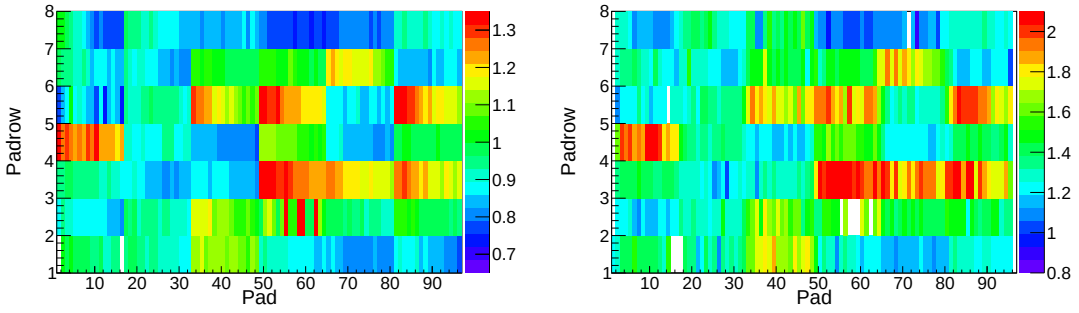

(A) Pulser gains (B) Krypton gains

FIGURE 5.1: Comparison of two gain maps for different calibration methods

The gain factors have a different scale because different pads were taken as reference pads in both methods. Nonetheless in both cases structures created on both maps are similar

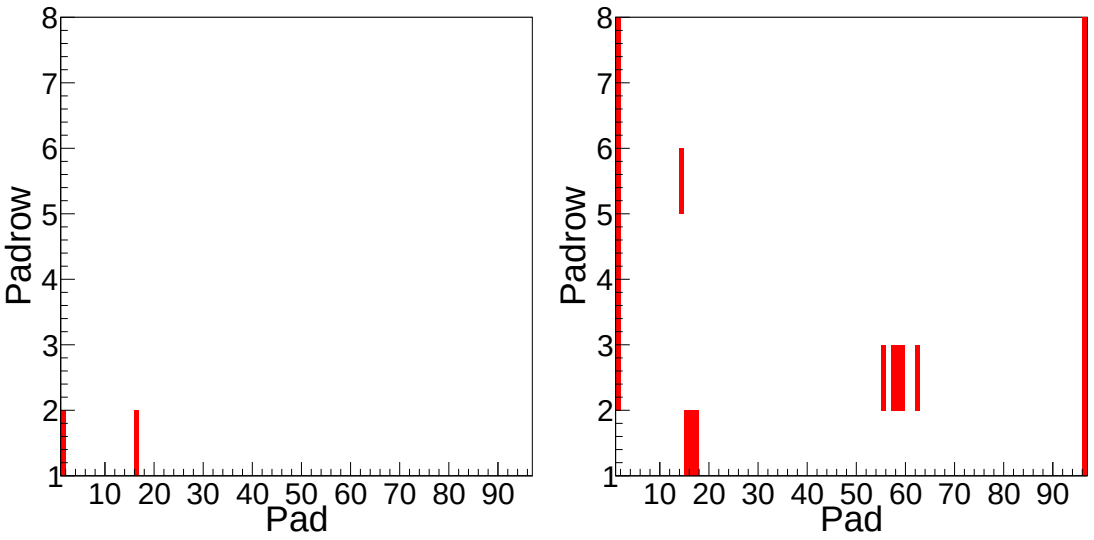

(A) Pulser gains (B) Krypton gains

FIGURE 5.2: Comparison of broken pads maps for different calibration methods

The krypton calibration is more narrow and therefore it rejects more pads. It is visible that all the broken pads from pulser calibration are present in the krypton calibration map.

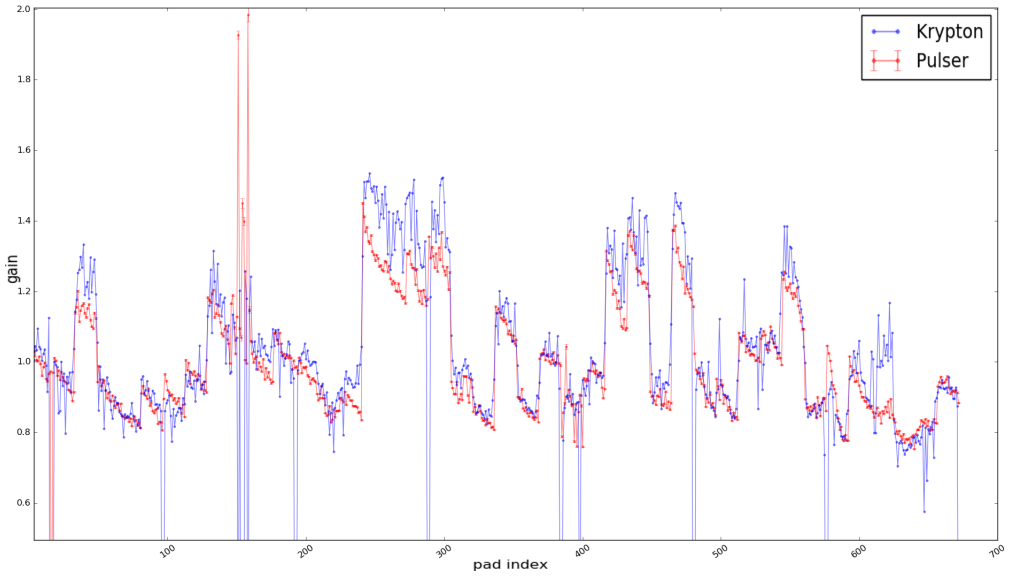

FIGURE 5.3: A plot showing comparison between two calibration methods

Once again the plot comparing two methods pad by pad, shows overall consistency.

5.3 Possible improvements

The Kr calibration software developed by me can still be improved as the whole process requires more of a sense of intuition than technical knowledge. The most important and awaited improvement is the introduction of a 3D cluster finder. The cluster finder currently used for calibration does not recognize charge leaks to other padrows. Such a situation can be imagined easily when an electron cloud hits the border of two padrows.

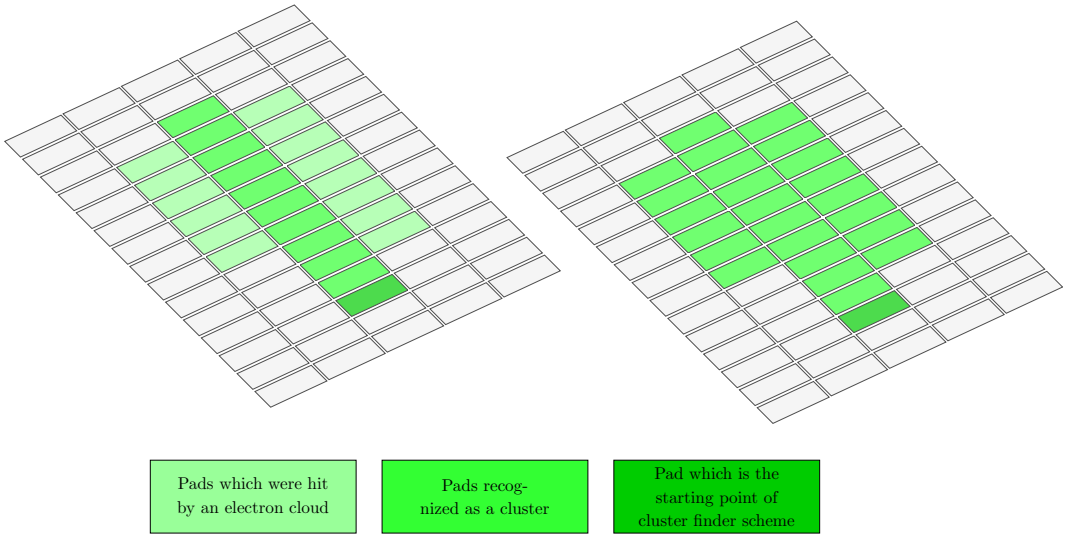

FIGURE 5.4: The difference between the cluster finder(on the left) and the 3D cluster finder is that the latter allows for charge leaks between padrows.

Appendix A

Pulser calibration

The pulser calibration is an alternative method of TPCs calibration. It is mostly used in order to obtain $t0$ time shifts and measure the response of electronics. As an addition it can be also used for gain calibration similarly as the krypton calibration.

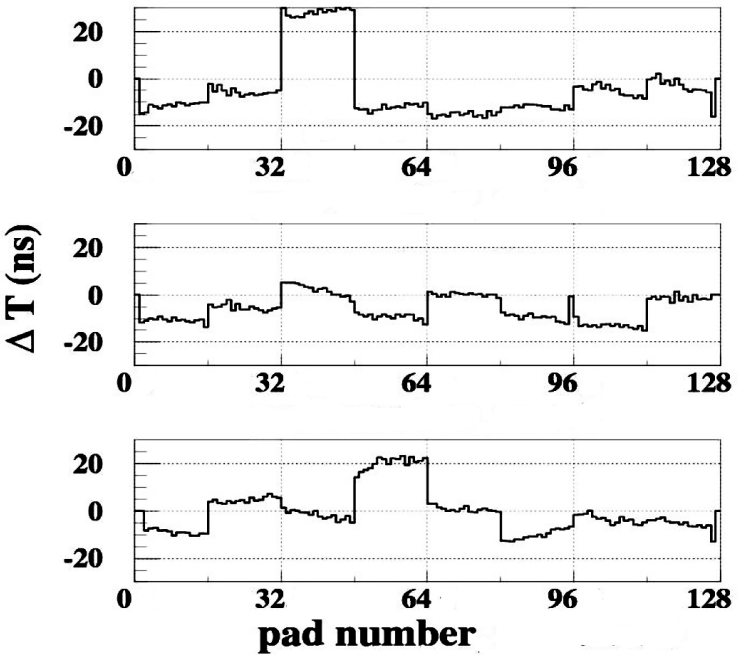

FIGURE A.1: Time delays for MTPC-L sector 2

Pulser is an electronic device that injects a charge in form of the step function like signal into the cathode wires. This should cause a gaussian-shaped response of the electronics in the pad plane.

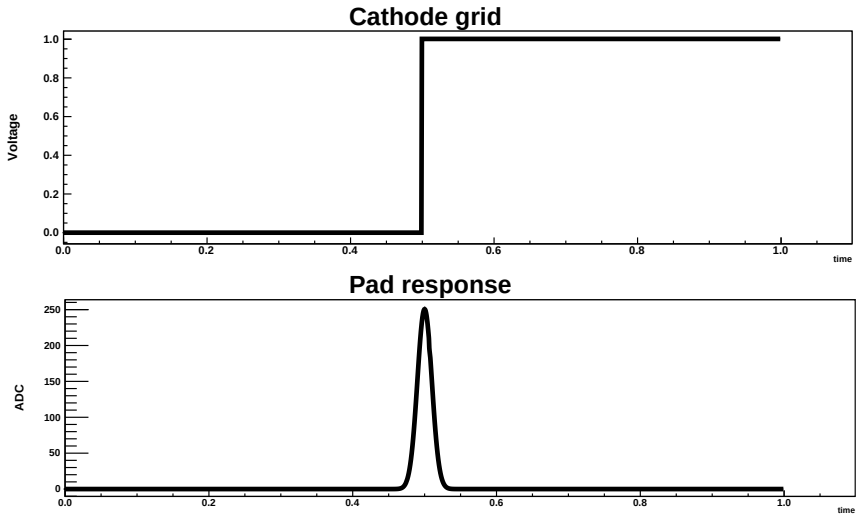

FIGURE A.2: Presentation of the theoretical pad response to the pulser signal

The real pad response to the signal looks different and includes a pedestal which is a standard background. Time shifts between pads are separated into two categories

- Chip to chip - trigger cable length variations (large)
- Pad to pad -shapeing time variations (small)

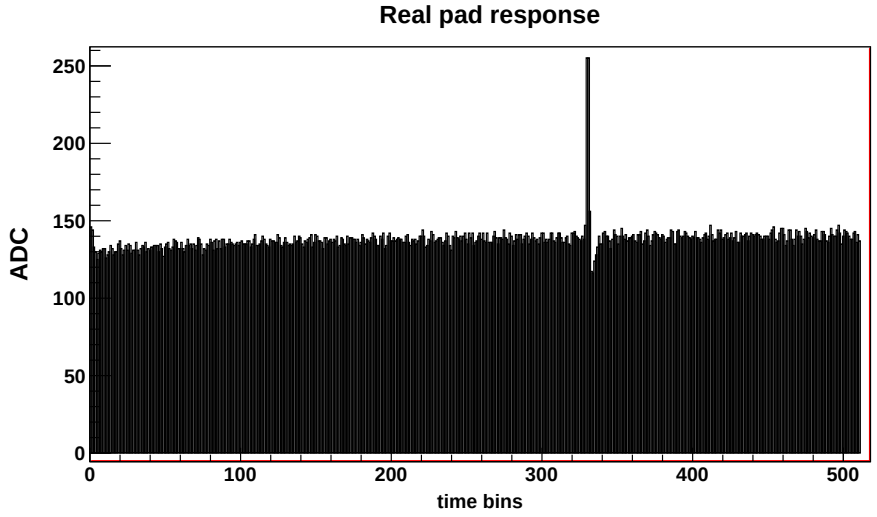

FIGURE A.3: Real response from pad

During the software development by Maciej Lewicki, two methods of fitting were examined. One included the damped oscillator function which should resemble the electronic

response. Nevertheless, the Gaussian fitting proved to be much more successful. The procedure consists of two steps. First we have to remove the pedestal background, then the fitting procedure can be applied.

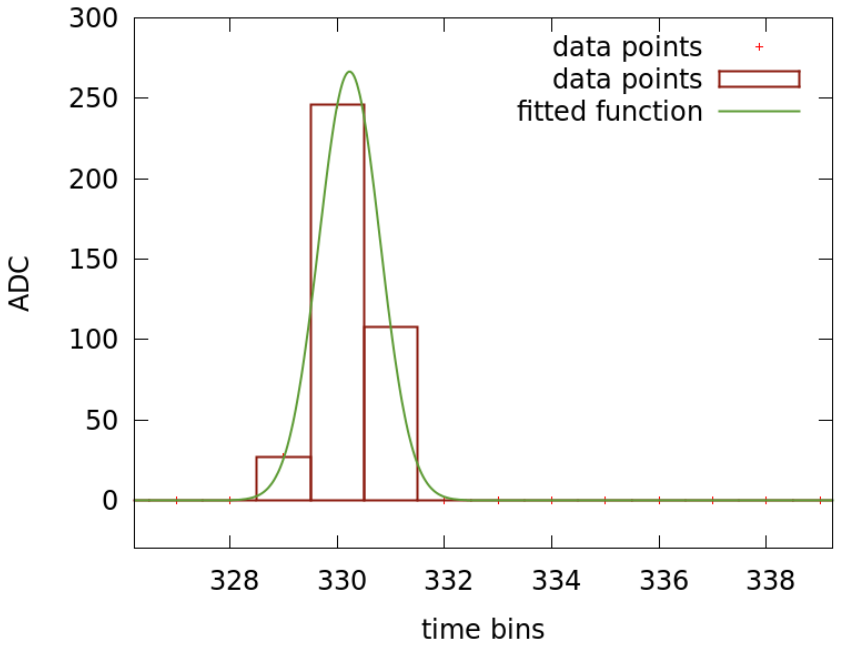

FIGURE A.4: The pedestal subtracted data with the Gaussian fit

The integrals over the Gaussian fits from the pedestal subtracted data are proportional to the electronics response of pads. Therefore we can use the integrals for calculating pad to pad gain factors. Gains obtained in this way can be used for cross check with different calibration methods as the krypton calibration.

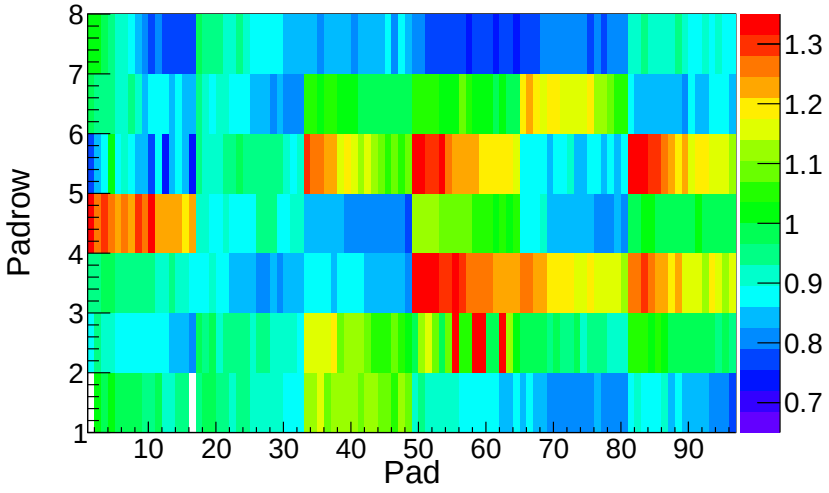

FIGURE A.5: Map of the gains for the GTPC obtained using the pulser calibration

Bibliography

[1] N. Abgrall et al. Na61/shine facility at the cern sps: beams and detector system. *JINST*, 9, June 2014. URL http://arxiv.org/abs/1401.4699.

[2] Antoni Aduszkiewicz. Operation and performance of time projection chambers of shine/na61 experiment at cern. *Master thesis*, June 2008.

[3] Andrzej Rybicki. Charged hadron production in elementary and nuclear collisions at 158 gev/c. *Ph.D. Dissertation*, March 2002.